RESEARCH ARTICLE

Open Access

Hypoxia and Foxn1 alter the proteomic signature of dermal fibroblasts to redirect scarless wound healing to scar-forming skin wound healing in Foxn1$^{-/-}$ mice

Barbara Gawronska-Kozak[1]* , Sylwia Machcinska-Zielinska[1], Katarzyna Walendzik[1], Marta Kopcewicz[1], Mirva Pääkkönen[2] and Joanna Wisniewska[1]

Abstract

Background Foxn1$^{-/-}$ deficient mice are a rare model of regenerative skin wound healing among mammals. In wounded skin, the transcription factor Foxn1 interacting with hypoxia-regulated factors affects re-epithelialization, epithelial-mesenchymal transition (EMT) and dermal white adipose tissue (dWAT) reestablishment and is thus a factor regulating scar-forming/reparative healing. Here, we hypothesized that transcriptional crosstalk between Foxn1 and Hif-1α controls the switch from scarless (regenerative) to scar-present (reparative) skin wound healing. To verify this hypothesis, we examined (i) the effect of hypoxia/normoxia and Foxn1 signalling on the proteomic signature of Foxn1$^{-/-}$ (regenerative) dermal fibroblasts (DFs) and then (ii) explored the effect of Hif-1α or Foxn1/Hif-1α introduced by a lentiviral (LV) delivery vector to injured skin of regenerative Foxn1$^{-/-}$ mice with particular attention to the remodelling phase of healing.

Results We showed that hypoxic conditions and Foxn1 stimulation modified the proteome of Foxn1$^{-/-}$ DFs. Hypoxic conditions upregulated DF protein profiles, particularly those related to extracellular matrix (ECM) composition: plasminogen activator inhibitor-1 (Pai-1), Sdc4, Plod2, Plod1, Lox, Loxl2, Itga2, Vldlr, Ftl1, Vegfa, Hmox1, Fth1, and F3. We found that Pai-1 was stimulated by hypoxic conditions in regenerative Foxn1$^{-/-}$ DFs but was released by DFs to the culture media exclusively upon hypoxia and Foxn1 stimulation. We also found higher levels of Pai-1 protein in DFs isolated from Foxn1$^{+/+}$ mice (reparative/scar-forming) than in DFs isolated from Foxn1$^{-/-}$ (regenerative/scarless) mice and triggered by injury increase in Foxn1 and Pai-1 protein in the skin of mice with active Foxn1 (Foxn1$^{+/+}$ mice). Then, we demonstrated that the introduction of Foxn1 and Hif-1α via lentiviral injection into the wounded skin of regenerative Foxn1$^{-/-}$ mice activates reparative/scar-forming healing by increasing the wounded skin area and decreasing hyaluronic acid deposition and the collagen type III to I ratio. We also identified a stimulatory effect of LV-Foxn1 + LV-Hif-1α injection in the wounded skin of Foxn1$^{-/-}$ mice on Pai-1 protein levels.

Conclusions The present data highlight the effect of hypoxia and Foxn1 on the protein profile and functionality of regenerative Foxn1$^{-/-}$ DFs and demonstrate that the introduction of Foxn1 and Hif-1α into the wounded skin of regenerative Foxn1$^{-/-}$ mice activates reparative/scar-forming healing.

Keywords Hypoxia, Foxn1, Pai-1, Skin wound healing, Dermal fibroblasts, Regeneration

*Correspondence:
Barbara Gawronska-Kozak
b.kozak@pan.olsztyn.pl
Full list of author information is available at the end of the article

Gawronska-Kozak *et al. BMC Biology*   (2024) 22:193

Page 2 of 28

Background

The major goal of skin wound healing is to reestablish its continuity to maintain the protective barrier role of the cutis. However, a fast and very efficient reparative method of healing, which culminates as a collagenous scar, does not allow the restoration of other functions for skin as an endocrine and sensory organ. Regenerative (scar-free) skin wound healing, which reestablishes skin appearance and functionality as intact skin, is common for mammalian embryos during the first 2/3 of in utero life but is seldom observed in adult mammals [1].

One of the rare examples of organisms having the ability to regenerate skin wounds in adulthood is Foxn1-deficient mice [2–4]. Foxn1 is a transcription factor expressed in epithelial cells of the skin and thymus [5, 6]. Inactivating mutation of Foxn1 results in a nude phenotype manifested by inborn thymus dysgenesis, lack of T-lymphocytes, macroscopic hairlessness and abnormal nail development [7]. In the skin, Foxn1 expression is restricted to the epidermis [6, 8]. Foxn1-positive keratinocytes are localized to the suprabasal layer and some cells of the basal layer where Foxn1 initiates keratinocyte differentiation, regulating the transition from a proliferative to a postmitotic stage and inducing the proliferation of neighbouring cells/keratinocytes to replace the differentiating population that exits the pool of progenitor cells [6]. However, in postwounded skin Foxn1 activity in epidermis also affects dermal part as our previous data showed [8–11]. During skin wound healing, Foxn1-positive cells regulate re-epithelialization, participate in the epithelial-mesenchymal transition (EMT) process and affect dermal white adipose tissue (dWAT) homeostasis [8–11].

Hypoxia is one of the factors that govern reparative vs regenerative skin wound healing stimulating proliferation, migration and angiogenesis [12–16]. Oxygen stress initiated by injury stimulates and stabilizes the expression of the transcription factor hypoxia-inducible factor-1α (Hif-1α), which orchestrates the restoration of cellular homeostasis in the hypoxic environment. Hif-1α impacts all stages of wound healing: inflammation, proliferation and remodelling. Its deficiency leads to the formation of nonhealing ulcers, whereas its overexpression has been associated with fibrotic diseases [17]. Interestingly, differences in Hif-1α expression have already been detected between reparative healed tissues (adult skin) and privileged for regenerative healing foetal skin [12]. The postwounded skin of mammalian foetuses (sheep) that healed in a regenerative manner showed no Hif-1α expression. In contrast, an increase in Hif-1α expression was detected in postwounded adult sheep skin that heals in a scar-forming, reparative manner [12]. Machcinska et al. recently reported that postwounded skin of Foxn1$^{-/-}$ mice (regenerative model of skin wound

healing) in terms of hypoxia-regulated factors revealed very low expression of Hif-1α that was unaffected by wounding and stable expression of Fih-1 (a factor inhibiting Hif-1α) that was unchanged by wounding [4]. In contrast, the skin of Foxn1$^{+/+}$ mice displayed an increase in Hif-1α and a decrease in Fih-1 in response to excisional wounds [4]. The data suggest that Foxn1 (Foxn1$^{+/+}$ mice), as a potential regulator of Hif-1α, governs the reparative (scar-present) skin wound healing process. Our recent data also showed that Foxn1 in keratinocytes, particularly under a hypoxic environment, affects epidermal reconstruction after injury and defined Foxn1 in keratinocytes as an important regulator in antioxidant defense [18].

Dermal fibroblasts (DFs) in the course of skin wound healing regulate the release of signal molecules and the production and modulation of extracellular matrix (ECM) components to affect the final outcome of the process: scar-free (regeneration) or scar-present (reparation). DFs are a diverse population of cells. Their diversity is related to their localization in skin (intrasite); there are papillary, reticular and dermo-hypodermal junction fibroblasts [19, 20], which have different embryonic origins that reflect anatomical locations within the body (e.g. head vs. trunk/torso) [21]. Rinkevich et al. revealed the existence of two populations of DFs in the dorsal skin of mice: EPFs (Engrailed-1-lineage-positive fibroblasts) and ENFs (En1-lineage negative fibroblasts), whose abundance dictates the outcome of healing: scar-free for ENFs or scar-present for EPFs [22, 23]. These researchers also demonstrated that the outcome of wound healing, scar-free or scar-present, is related to intrinsic differences among DFs manifested by different ECM components and cytokines/growth factors/enzymes production/turnover but not the local environment. These studies helped elucidate the diversity in DF populations. However, there are limited data on the factors that determine DF signatures to guide them to particular niches/functions within the skin. These factors include AP-1 and genes that are under AP-1 control [24, 25], Wnt pathways [26] and Yap signalling [27, 28].

During our investigations, we showed that Foxn1 inactivity in the skin (Foxn1$^{-/-}$ mice) results in distinctive DF characteristics [29, 30]. DFs isolated from regenerative Foxn1$^{-/-}$ mice were characterized by a higher percentage of cells with stem cell markers (CD117 and Oct3/4), higher expression of matrix metalloproteinases (Mmp 3, 9, 13), collagen type III and Tgfβ3 transcripts and higher levels of hyaluronic acid than those derived from Foxn1+/+ mice. Similar characteristics of DFs were shown for other regenerative models, such as mammalian foetuses [31], and for gingival/oral fibroblasts privileged for scar-free healing [32].

Gawronska-Kozak *et al. BMC Biology*   (2024) 22:193

Page 3 of 28

Skin wound healing, whether regenerative or reparative, comprises three defined and overlapping stages: (i) inflammation, (ii) new tissue generation (proliferation and migration of keratinocytes and fibroblasts) and (iii) remodelling. The outcome of the healing process, scar vs. no-scar, has been related to the magnitude of response (e.g. levels of inflammatory response), the ratio of pro- to antiscarring factors (e.g. MMPs/TIMPs; TGFβ1/TGFβ3) and the levels and timing of factors released to pericellular/extracellular postwounded tissues (e.g. hyaluronic acid, collagens) [33]. The final structure of postwounded tissues is achieved through the synthesis of structural elements of the ECM, such as collagens, hyaluronic acid, glycosaminoglycans that replace the provisional matrix (fibrin) and enzymes that degrade and modulate the ECM and participate in ECM-cell communication. DFs are the central effector cells that direct the composition of the postwounding matrix through synthesis, accumulation, degradation and remodelling to act as key mediators of scarring [34].

In the present study, we hypothesized that transcriptional crosstalk between Foxn1 and Hif-1α controls the switch from scarless (regenerative) to scar-present (reparative) skin wound healing. To verify this hypothesis, we examined (i) the effect of hypoxia/normoxia and Foxn1 signalling on the Foxn1$^{-/-}$ (regenerative) DF proteomic signature and then (ii) explored the effect of Hif-1α or Foxn1/Hif-1α introduced by a lentiviral (LV) delivery tool to postinjured skin of regenerative Foxn1$^{-/-}$ mice with particular attention to the remodelling phase of healing.

Results

Proteomic profile of DFs and DF conditioned media (DFCM) exposed to hypoxic (1% O$_2$) or normoxic (21% O$_2$) conditions

Our previous study showed that Ad-Foxn1 transduced into keratinocytes increases the expression of Foxn1 and stimulate Foxn1 activity which manifest by (i) an increase in the percentage of keratin 10 (marker of differentiated keratinocytes) positive keratinocytes, (ii) upregulation of involucrin (the late marker of keratinocyte differentiation) and keratin 16 (keratinocyte activation) proteins, (iii) suppression of the levels of phospho-PKC (pan), which is recognized as a downstream target of Foxn1 [35]. We also showed that Foxn1 (Ad-Foxn1 transduced into keratinocytes) and hypoxia profoundly change keratinocyte proteomic characteristics that affect keratinocyte functionality: migration, proliferation and the antioxidant defense system [18]. In the present study, we explored whether DFs isolated from Foxn1$^{-/-}$ mice (regenerative model) upon hypoxia and/or Foxn1 stimulation alter the protein profiles to those characteristic of reparative/proscarring healing.

DFs isolated from regenerative Foxn1$^{-/-}$ mice were cocultured with keratinocytes transduced with adenovirus carrying Foxn1 (Ad-Foxn1+GFP) or GFP (Ad-GFP, control) under hypoxic or normoxic conditions for 24 h (Fig. 1). In total, 4941 proteins were identified from DFs grown under normoxic conditions, and 4833 proteins were identified from DFs grown under hypoxic conditions. When DFCM was collected under normoxic growth conditions, a total of 2362 proteins were identified compared to 2270 proteins from hypoxic conditions.
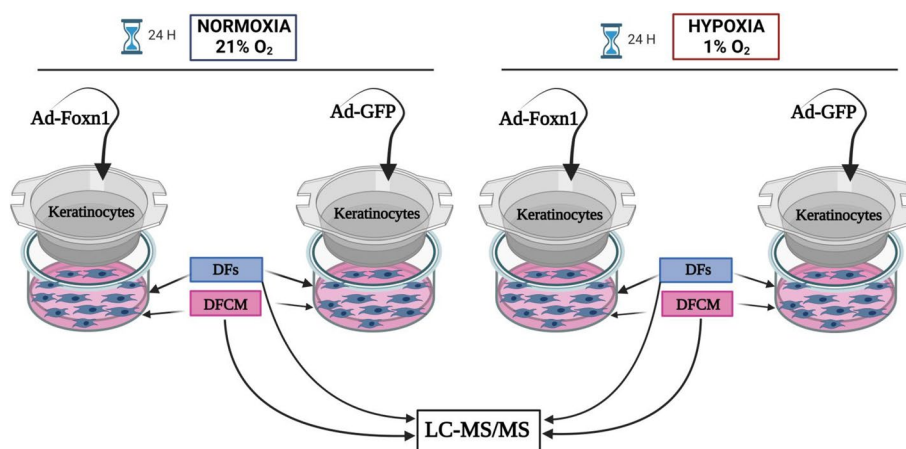
Fig. 1 Scheme of the proteomic experiment. DFs collected from the Foxn1$^{-/-}$ (CBy. Cg-Foxn1 < nu >/cmdb) mice were cocultured with keratinocytes collected from Foxn1.$^{+/+}$ (C57BL/6 J) mice. Keratinocytes seeded in inserts were transduced with adenovirus carrying Foxn1 (Ad-Foxn1) or control (Ad-GFP). Keratinocytes and DFs were cocultured under hypoxic (1% O$_2$) or normoxic (21% O$_2$) conditions (n=3, 2 animals per experiment, total n=6 animals). After 24 h of coculture, DFs and DFCM were collected separately and subjected to detailed mass spectrometry analysis (LC−MS/MS)

Gawronska-Kozak *et al. BMC Biology*   (2024) 22:193

Page 4 of 28

The collected DFs and DFCM underwent detailed proteomic analysis, and the mass spectrometry data have been deposited in the Proteomics Identifications Database (PRIDE) [36].

The LC−MS/MS data were searched against the Mus musculus database (SwissProt version 2019_10). For fold change analysis, log2-ratio values were filtered by a q-value (multiple testing corrected *p* value) of 0.05 and an absolute log2 ratio of 0.58 by default for all analyses (see "Methods"). The obtained data are presented as a set of DFs (Additional file 1: Tables S1-S2) or DFCM (Additional file 1: Tables S3-S4) proteins with differentially up- or downregulated expression under hypoxic vs. normoxic culture conditions. The analysis revealed that hypoxic vs. normoxic conditions differentially regulated 206 proteins in DFs cocultured with Ad-Foxn1-transduced keratinocytes (89 upregulated and 117 downregulated) and 209 in DFs cocultured with Ad-GFP keratinocytes (102 upregulated and 107 downregulated) (Table 1, Additional file 1: Tables S1-S2). The corresponding conditioned media showed 18 differentially regulated proteins upon hypoxia vs. normoxia with Ad-Foxn1 (15 up and 3 down) and 70 with Ad-GFP cocultured keratinocytes (57 up and 13 down) (Table 1, Additional file 1: Tables S3-S4).

Next, differentially expressed proteins detected in DFs (Table 1, Additional file 1: Tables S1-S2) or DFCM (Table 1, Additional file 1: Tables S3-S4) upon hypoxic/normoxic conditions and Ad-Foxn1/Ad-GFP keratinocyte coculture were analysed with Gene Ontology (GO) enrichment analysis to determine their potential functional classification.

Genes were categorized into five main GO categories: "Molecular function", "Biological processes", "Cellular components", "Protein class" and "Pathways", separately for DFs (Fig. 2, Additional file 2: Fig. S1) and DFCM (Fig. 3, Additional file 2: Fig. S2) using the PANTHER Classification System. Within the molecular function category, DF proteins involved in catalytic activity represented the major group that was highly regulated under hypoxic conditions: 53.1% upon coculture with Ad-Foxn1-keratinocytes and 48.3% upon coculture with Ad-GFP-keratinocytes (Fig. 2A,B). The molecular function category revealed a group of DF proteins involved in ECM deposition/remodelling regulated upon hypoxia that included Pai-1 and Loxl2, which were upregulated, and Adamts1 and Adamts5, which were downregulated in both Ad-Foxn1- and Ad-GFP-transduced keratinocyte cocultures (Fig. 2A,B).

Next, the possible interactions among DF proteins enriched by hypoxia/Ad-Foxn1-keratinocyte vs. hypoxia/Ad-GFP-keratinocyte cocultures, which were distinguished by the Panther classification system, were examined (Fig. 2C-D). With network models deposited in the STRING database [36], two separate networks of DF-interacting proteins stimulated by hypoxia/Ad-Foxn1 or hypoxia/Ad-GFP were established (Fig. 2C,D). Deposition of 206 (DFs cocultured with Ad-Foxn1 keratinocytes) or 209 (DFs cocultured with Ad-GFP keratinocytes) hypoxia-regulated proteins into the STRING database created networks of interconnected proteins. The large group of hypoxia-regulated proteins that were included in the networks is linked to ECM organization/modelling (Fig. 2C) and the proteins interacting with ECM (Fig. 2D). ECM-associated proteins allowed us to create separate heatmaps for the DF/Ad-Foxn1-keratinocyte coculture and DF/Ad-GFP-keratinocyte coculture, showing prot+eins that were up- or downregulated upon hypoxia (Fig. 2C,D). Hypoxia upregulated Pai-1, Sdc4, Plod2, Plod1, Lox, Loxl2, Itga2, Vldlr, Ftl1, Vegfa, Hmox1, Fth1, and F3 and downregulated the Adamts1, Adamts5, Thbs1, Thbs2, Traf2, Pdgfra, Il6st, and Stat1 proteins, which are common to Ad-Foxn1-keratinocyte and Ad-GFP-keratinocyte cocultures. Upregulation of Col16a1, Col3a1, Nos2, Gpc1, and Ccn2 and downregulation of Spp1, Col8a1, Loxl3, Csgalnact1, Bgn, Lmo4, Rnf213, Bcar1, Tnfrsf11b, Slit2, and Ldlr were detected exclusively in DFs cocultured with Ad-Foxn1 keratinocytes upon hypoxia (Fig. 2C,D).

Table 1 Number of proteins identified in DFs or DFCM that are differentially regulated after 24 h of exposure to hypoxic (1% O_2) or normoxic (21% O_2) conditions. DFs were isolated from Foxn1$^{−/−}$ (CBy. Cg-Foxn1 < nu >/cmdb) mice and cocultured with Ad-Foxn1- or Ad-eGFP-transduced keratinocytes

	Number of proteins differently regulated upon hypoxia vs normoxia culture conditions			
Co-cultured with Ad-Foxn1 transduced keratinocytes	DFs (total 206)		DFCM (total 18)	
	Upregulated	Downregulated	Upregulated	Downregulated
	89	117	15	3
Co-cultured with Ad-GFP transduced keratinocytes	DFs (total 209)		DFCM (total 70)	
	Upregulated	Downregulated	Upregulated	Downregulated
	102	107	57	13
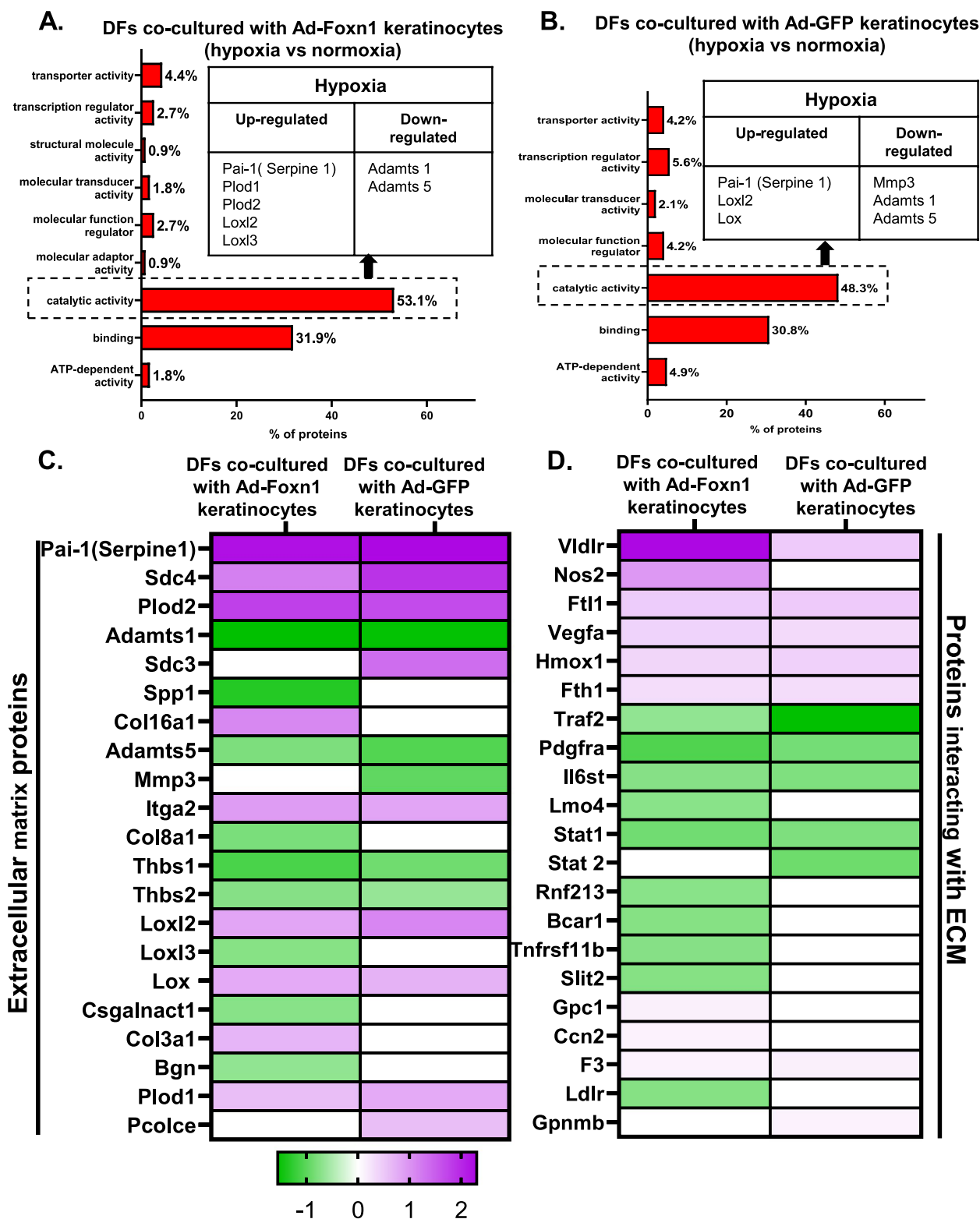
Fig. 2 Classification of DF proteins regulated upon hypoxia (1% O_2) vs. normoxia (21% O_2) that were cocultured with Ad-Foxn1 (**A**)- or Ad-GFP (**B**)-transduced keratinocytes for 24 h according to GO using PANTHER and enriched with the g: Profiler database. **A, B** Diagrams illustrate detected proteins in terms of "molecular function" (with detailed proteins included in the catalytic activity class). **C, D** Heatmap of DF proteins linked to ECM organization (**C**) or the proteins interacting with ECM (**D**) enriched by hypoxia separately for coculture with Ad-Foxn1 or Ad-GFP keratinocytes. The scale bar in the heatmap indicates protein fold changes ranging from +12 to −1

Gawronska-Kozak *et al. BMC Biology*　(2024) 22:193

Page 6 of 28
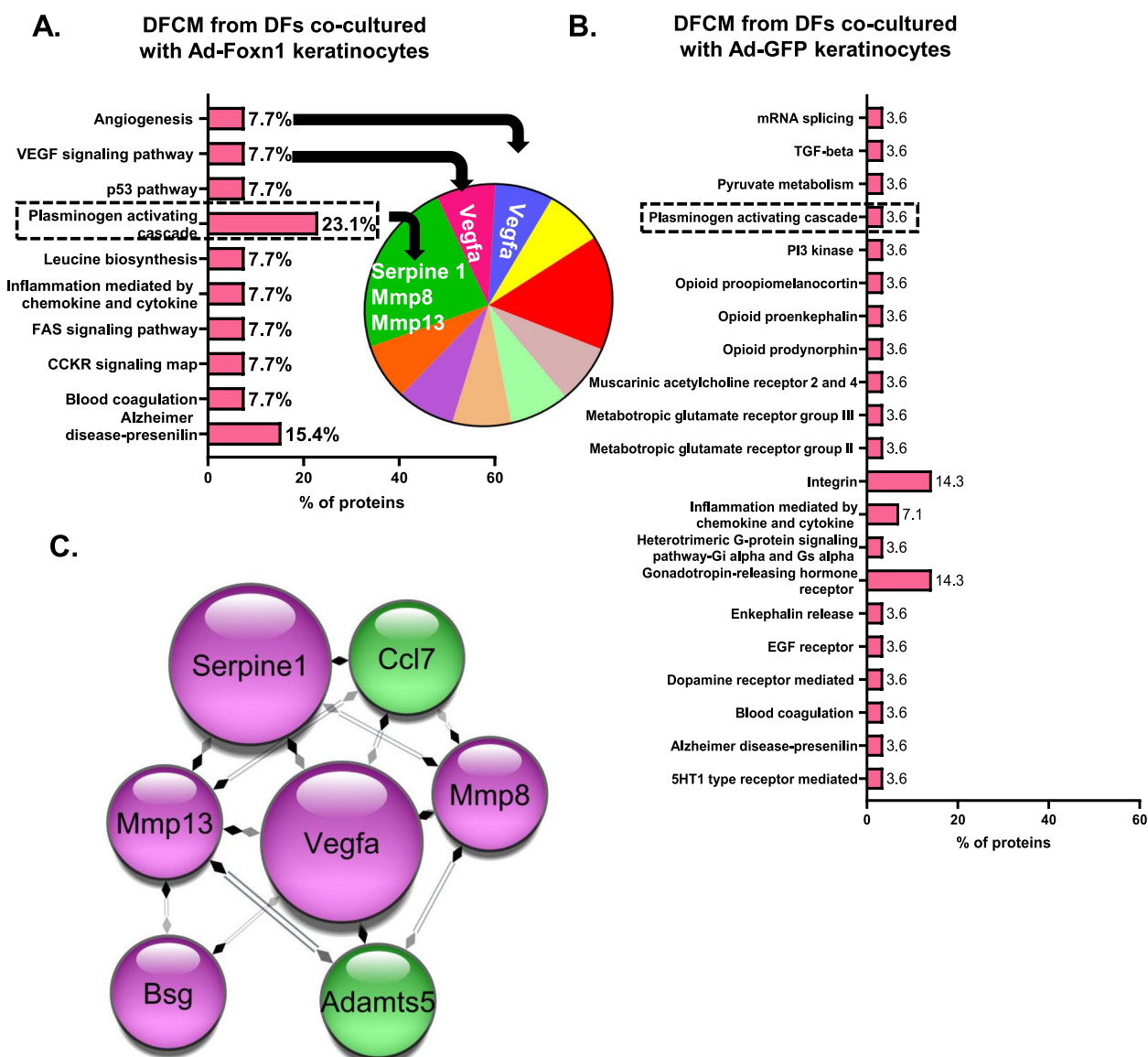
Fig. 3 Classification of proteins identified in DFCM regulated upon hypoxia (1% O_2) vs. normoxia (21% O_2) for keratinocytes transduced with Ad-Foxn1 (**A**) or Ad-GFP (**B**). Diagrams illustrate detected proteins in terms of the "Pathway" category with detailed proteins included in the plasminogen activating cascade. **C** Interactive network of proteins up- (Pai-1, Mmp-13, Mmp-8, Vegfa, Bsg) or downregulated (Ccl7 and Adamts5) in the DFCM from DFs cocultured with Ad-Foxn1 keratinocytes

Next, we analysed proteins released into culture media (DFCM) upon hypoxia, separately for Ad-Foxn1- or Ad-GFP-keratinocyte coculture (Table 1, Additional file 1: Tables S3-S4). Generally, the analysis showed similarities between DFCM with Ad-Foxn1 or Ad-GFP-keratinocyte coculture within the biological process, cellular component, protein class and molecular function categories (Additional file 2: Fig. S2).

However, the analysis of DFCM proteins within the "Pathways" category showed differences upon Ad-Foxn1-keratinocyte vs. Ad-GFP-keratinocyte coculture,

particularly between those involved in the plasminogen activating cascade pathway (Fig. 3). DFCM collected from hypoxic, Ad-Foxn1-keratinocyte-stimulated cocultures showed enrichment up to 23.1% for proteins involved in the plasminogen activating cascade pathway, whereas hypoxic and Ad-GFP showed enrichment up to 3.6% (Fig. 3A,B).

Of interest, exclusively DFCM from hypoxia and Ad-Foxn1-keratinocyte coculture had Pai-1 and Mmp8 protein within the plasminogen activating cascade pathway, but they were not present in DFCM upon

Ad-GFP-keratinocyte coculture (Additional file 1: Tables S3-S4). DFCM proteins that were distinguished upon hypoxia and Ad-Foxn1-keratinocyte coculture formed an interactive network of upregulated Pai-1, Mmp-13, Mmp-8, Vegfa, and Bsg and downregulated Ccl7 and Adamts5 proteins (Fig. 3C).

The effect of Tgfβ1 or Tgfβ3 on DFs isolated from the skin of regenerative (Foxn1$^{-/-}$) or reparative (Foxn1$^{+/+}$) mice

The proteomic data showed that hypoxia stimulates DFs to synthesize proteins involved in ECM organization and modelling (see Fig. 2). Intriguingly, Pai-1, the protein known to stimulate fibrosis, was upregulated upon hypoxia in DFs cocultured with Ad-Foxn1- and Ad-GFP-keratinocytes (Fig. 2) but released into DFCM exclusively upon Ad-Foxn1-keratinocyte stimulation (Fig. 3). Therefore, in the next step of our investigation, we compared Pai-1 levels in DFs isolated from Foxn1$^{+/+}$ mice (reparative) to DFs from Foxn1$^{-/-}$ (regenerative) mice (Fig. 4, Additional file 2: Fig. S3, Fig. S4). We also applied Tgfβ as an established stimulator of Pai-1 expression (Fig. 4, Additional file 2: Fig. S3, Fig. S4).

Western blot followed by densitometric analyses showed high levels of Pai-1 in DFs isolated from Foxn1$^{+/+}$ mice (Fig. 4A,B; $p < 0.05$) compared with Foxn1$^{-/-}$ DFs. Cultured DFs were also stimulated with Tgfβ1 or Tgfβ3 for 24 h. The differences in Pai-1 levels that were already observed in control, nonstimulated cultures were further evident after Tgfβ treatment (Fig. 4A,B). Regardless of Tgfβ1 or Tgfβ3 stimulation, Pai-1 levels were always higher in Foxn1$^{+/+}$ than in Foxn1$^{-/-}$ DFs. Interestingly, the stimulatory effect of Tgfβ3 on Pai-1 accumulation was much more pronounced than that of Tgfβ1 in Foxn1$^{+/+}$ DFs ($p < 0.001$) and Foxn1$^{-/-}$ DFs ($p < 0.05$) (Fig. 4A,B).

Vegfa was also identified in DFCM collected from DFs cocultured with Ad-Foxn1 but not Ad-GFP (control)-transduced keratinocytes (see Fig. 3A, C, Additional file 1: Tables S3-S4). Therefore, we next explored whether there are in situ differences between Foxn1$^{+/+}$ DFs and Foxn1$^{-/-}$ DFs related to Vegfa protein levels. Western blot followed by densitometric analyses showed no differences in Vegfa protein levels between DFs isolated from Foxn1$^{+/+}$ or Foxn1$^{-/-}$ mice regardless of whether they were controls or treated with Tgfβ1 or Tgfβ3 (Fig. 4C,D). A stimulatory effect on Vegfa protein levels was exclusively detected for Tgfβ3 affecting both Foxn1$^{-/-}$ and Foxn1$^{+/+}$ DFs (Fig. 4C,D).

Hypoxia/normoxia and/or Ad-Foxn1/Ad-GFP culture conditions affect Foxn1$^{-/-}$DF functional characteristics

The detected changes in the DF proteomic profile, particularly those related to culture conditions, motivated us to examine how hypoxia vs. normoxia modifies the functional features of Foxn1$^{-/-}$ DFs (Fig. 5, Additional file 2: Fig. S5). We analysed the proliferation, migration and metabolic activity of DFs through BrdU (Fig. 5A), MTT (Fig. 5B), and scratch (Fig. 5C, Additional file 2: Fig. S5) in vitro assays. For the in vitro assays, monolayered Foxn1$^{-/-}$ DFs were cultured under normoxia or hypoxia with conditioned media (keratinocyte conditioned media; KCM) collected from Ad-Foxn1- or Ad-eGFP-transduced keratinocytes.

The proliferative potential of Foxn1$^{-/-}$ DFs was inhibited by hypoxia (1% oxygen availability) ($p < 0.01$) regardless of whether KCM from Ad-Foxn1- or Ad-eGFP-transduced keratinocytes was used for DF culture (Fig. 5A). Culture conditions related to oxygen availability or Foxn1 presence showed no effect on DF metabolic potential measured with the MTT assay (Fig. 5B). Foxn1$^{-/-}$ DFs displayed gradual migratory progress during the first 20–24 h, covering the gap between scratch edges (Fig. 5C). The migration of DFs was not affected by normoxia/hypoxia or conditioned culture media from Ad-Foxn1- or Ad-eGFP-transduced keratinocytes (Fig. 5C, Additional file 2: Fig. S5).

Foxn1 and Hif-1α lentiviral transgene delivery modify skin wound healing in Foxn1$^{-/-}$ mice

As a prerequisite for in vivo experiments, we examined LV-transduction efficiency and cell specificity in in vitro model. Primary cultures of keratinocytes (Fig. 6A,B) or DFs (Fig. 6C,D) isolated from newborn C57BL/6 mice were transduced with LV vectors carrying Foxn1 (Fig. 6A, C) or Hif-1α (Fig. 6B, D). The replicate experiments showed an increase in both Foxn1 mRNA and Hif-1α mRNA expression in keratinocytes transduced regardless with LV-Hif-1α or LV-Foxn1 (compare Fig. 6A, B). In contrast, only DFs transduced with LV-Foxn1 displayed extremely high expression of Foxn1 mRNA with no Foxn1 mRNA expression in non-transduced or LV-Hif-1α transduced DFs (Fig. 6C). This data confirmed epidermal-specific Foxn1 expression [6–8] but also showed the capacity of DFs to express Foxn1 mRNA after LV delivery. The increase in Hif-1α mRNA expression was detected exclusively in DFs transduced with LV-Hif-1α in comparison to stable and low levels of Hif-1α mRNA in LV-Foxn1 transduced or non-transduced DFs (Fig. 6D).

The present proteomics analysis (see Figs. 2 and 3) highlights that hypoxia together with Foxn1 signalling pathways stimulates proteins involved in ECM organization. Accordingly, we asked whether the introduction of LVs carrying Hif-1α or Hif-1α/Foxn1 into the wounded skin of Foxn1$^{-/-}$ mice at day 1 affects the skin wound healing process, particularly during the

A.

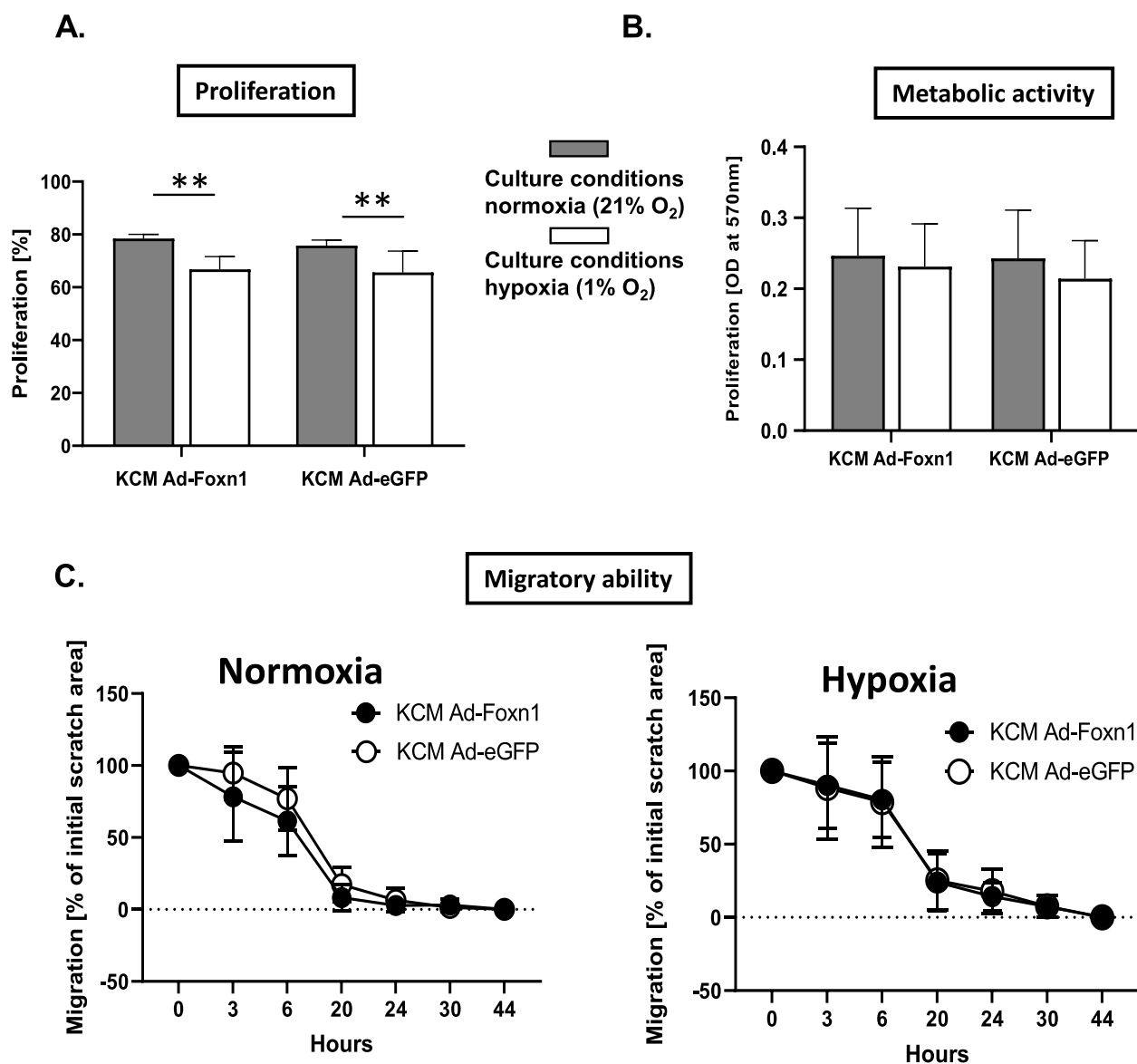**B.**

C.

D.
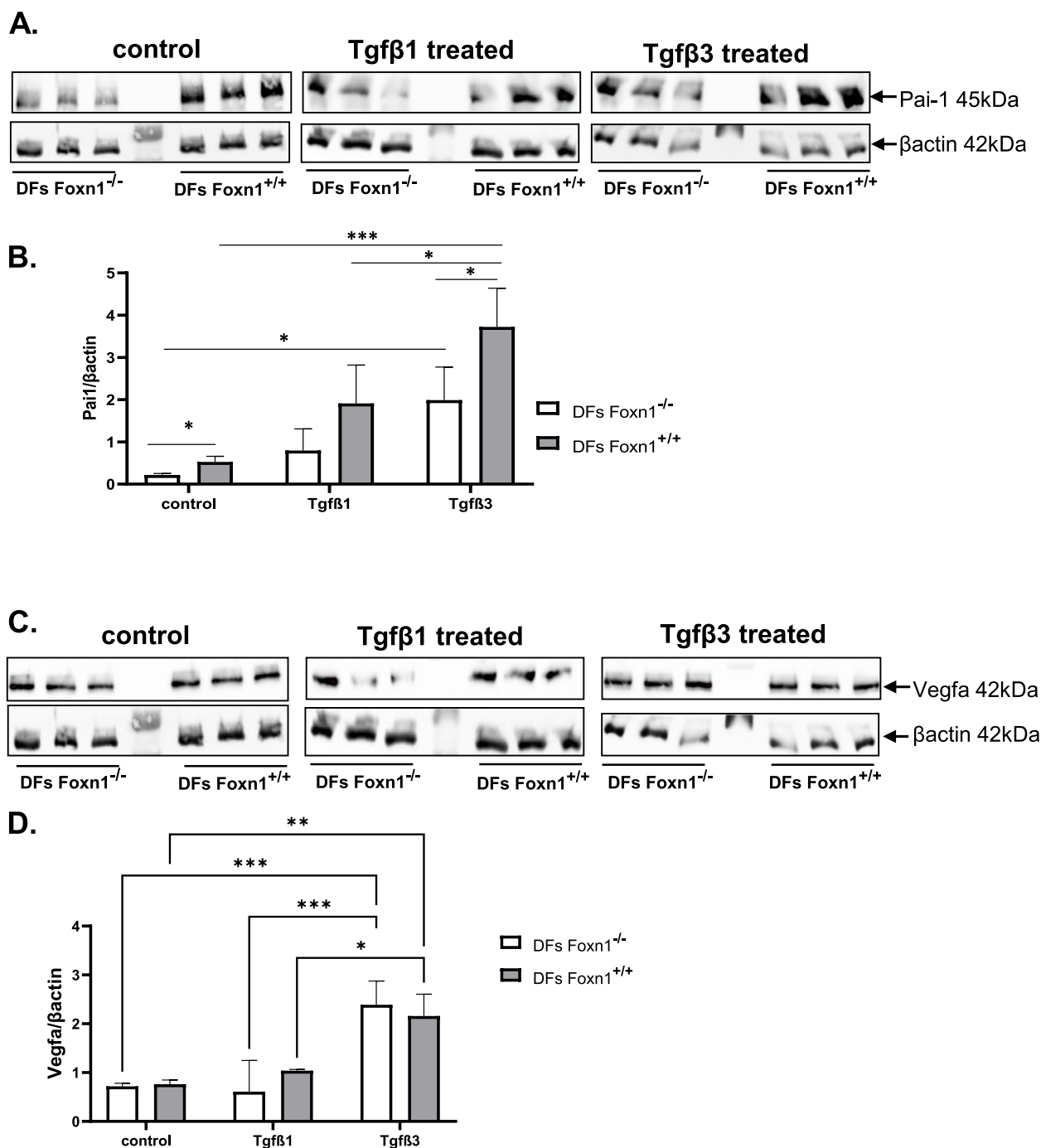
Fig. 4 Pai-1 (**A,B**) and Vegfa (**C,D**) protein levels in cultured DFs isolated from the skin of Foxn1^{+/+} or Foxn1.[−/−] mice. Western blots for control, Tgfβ1- or Tgfβ3-treated DFs (**A** and **C**) followed by densitometric analyses (**B** and **D**). Values are the lsmean ± SE; asterisks indicate significant differences (*$p < 0.05$; ** $p < 0.01$, *** $p < 0.001$)

remodelling phase at day 14 (Fig. 7A). There were no adverse effects of LV injection on mouse behaviour (personal observations) or body weight (Additional file 2: Fig. S6) during the experiment.
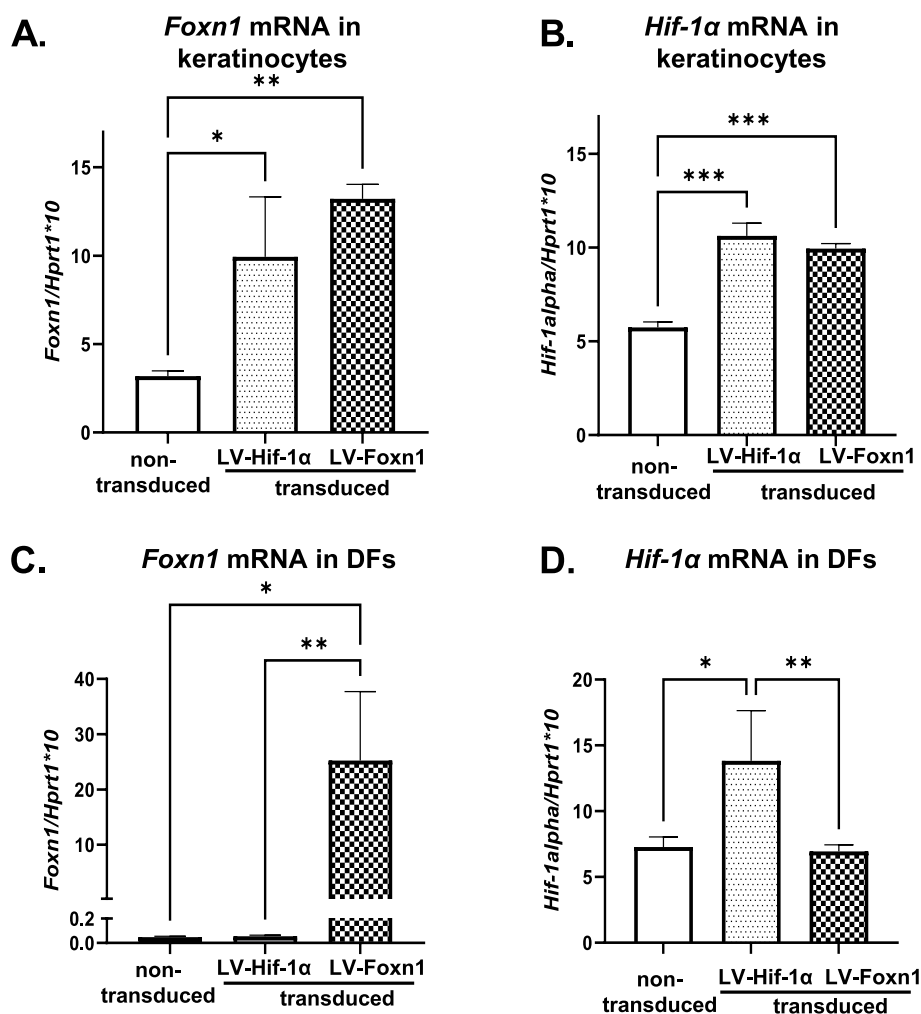
LV-transduction efficiency

First, applying flow cytometry analyses we estimated the LV transduction efficiency by measuring the percentage of eGFP (LV-eGFP or LV-Hif-1α-eGFP)- or mCherry

A.

Proliferation

Culture conditions
normoxia (21% O_2)

Culture conditions
hypoxia (1% O_2)

B.

Metabolic activity

C.

Migratory ability

Fig. 5 Oxygen availability (normoxia vs. hypoxia) modulates DFs: proliferation (**A**), metabolic activity (**B**) and migration (**C**). Foxn1.$^{-/-}$ DFs cultured under hypoxic or normoxic conditions with KCM (keratinocyte conditioned media) from Ad-Foxn1- or Ad-GFP-transduced keratinocytes were analysed with a BrdU incorporation assay followed by flow cytometry analysis (**A**; $n=4$), MTT metabolic activity assay (**B**; $n=4$) or scratch migratory assay (**C**; $n=4$). Values are the lsmean ± SE; asterisks indicate significant differences between normoxic or hypoxic condition transduction (**$p<0.01$)

(LV-Foxn1-mCherry)-positive cells isolated from the wounded skin of Foxn1$^{-/-}$ mice at day 14 that were LV-injected at day 1 (Fig. 7B). With antibodies against eGFP or mCherry protein, the highest percentage of transduced cells at postwounding day 14 was detected in the skin treated with both LV-Hif1α+LV-Foxn1, which consisted of 0.23% eGFP (Hif-1α), 3.4% mCherry (Foxn1) and 0.53% double-positive eGFP+mCherry cells (Hif-1α+Foxn1) (Fig. 7B). Flow cytometry analyses not only allow us to estimate the percentage of transduced skin cells but also to characterize

the phenotype. eGFP-, mCherry- or eGFP+mCherry-positive cells isolated at postwounding day 14 from the skin of LV-eGFP-, LV-Hif-1α- and LV-Foxn1+LV-Hif-1α-injected mice were characterized for E-cadherin (epidermal marker) or vimentin (dermal marker) positivity (Fig. 7C–E). The phenotypic analysis revealed that LV-Hif-1α was incorporated predominantly into E-cadherin (54.9%) and E-cadherin/Vimentin (42.725%) positive cells (Fig. 7D). Cells isolated from the skin of LV-Foxn1+LV-Hif-1α-injected mice showed the largest population of E-cadherin/Vimentin

Fig. 6 Transduction efficiency of LVs carrying Hif-1α-eGFP or Foxn1-mCherry in cell culture model. qRT-PCR analysis of Foxn1 (**A**, **C**) or Hif-1α (**B**, **D**) mRNA expression in keratinocytes (**A**, **B**) or DFs (**C**, **D**). Asterisks indicate significant differences (* $p < 0.05$; ** $p < 0.01$; *** $p < 0.001$). Data represent the mean ± SD

(59.85%) and E-cadherin (38,925%) positive cells (Fig. 7E). Vimentin expressing cells consists of less than 1% of positive cells regardless LV-Hif-1α (0.075%) or LV-Foxn1 + LV-Hif-1α (0.775%)-injected mice (Fig. 7D,E). Within whole isolated cells, the largest group was formed by E-cadherin-positive cells, followed by E-cadherin + Vimentin cells and then

vimentin-positive cells, regardless of LV-eGFP (Fig. 7C), LV- Hif-1α (Fig. 7D) or LV-Foxn1 + LV-Hif-1α (Fig. 7E) injection. Next, immunohistochemical detection assays for mCherry positivity were performed on postwounded and LV-Foxn1-mCherry-injected skin (Fig. 7F). Microscopic analysis of skin sections at day 6 after injury showed positive

(See figure on next page.)

Fig. 7 Transduction efficiency of LVs carrying eGFP (control), Hif-1α-eGFP or Foxn1-mCherry + Hif-1α-eGFP injected into the wounded skin of Foxn1$^{-/-}$ mice at postwounding day 1 analysed by flow cytometry at day 14 or by immunohistochemistry for mCherry (LV-Foxn1-mCherry) at postwounding day 6. **A** Scheme of experiment. **B** Percentage of cells positive for eGFP or mCherry isolated from the injured skin of LV-eGFP (control)-, LV-Hif-1α-eGFP- or LV-Hif-1α-eGFP + LV-Foxn1-mCherry-injected Foxn1$^{-/-}$ mice. **C–E** Percentage of E-cadherin (E-cad +), vimentin (Vim +) or E-cadherin + vimentin double-positive cells (E-cad/Vim +) within eGFP-positive (LV-eGFP or LV-Hif-1α) or mCherry + eGFP-positive (LV-Hif-1α + LV-Foxn1) populations in comparison to the whole cell population. **F** Immunohistochemical detection of mCherry (LV-Foxn1-mCherry) localization in the skin of Foxn1.$^{-/-}$ mice. Asterisks indicate significant differences (* $p < 0.05$; ** $p < 0.01$; *** $p < 0.001$; **** $p < 0.0001$). Data represent the mean ± SD. E-epidermis, D-dermis, arrowheads indicate positivity in epidermis, arrows point out positivity in dermis (**F**). Scale bar (F) 50 μm, (inset; 20 μm)
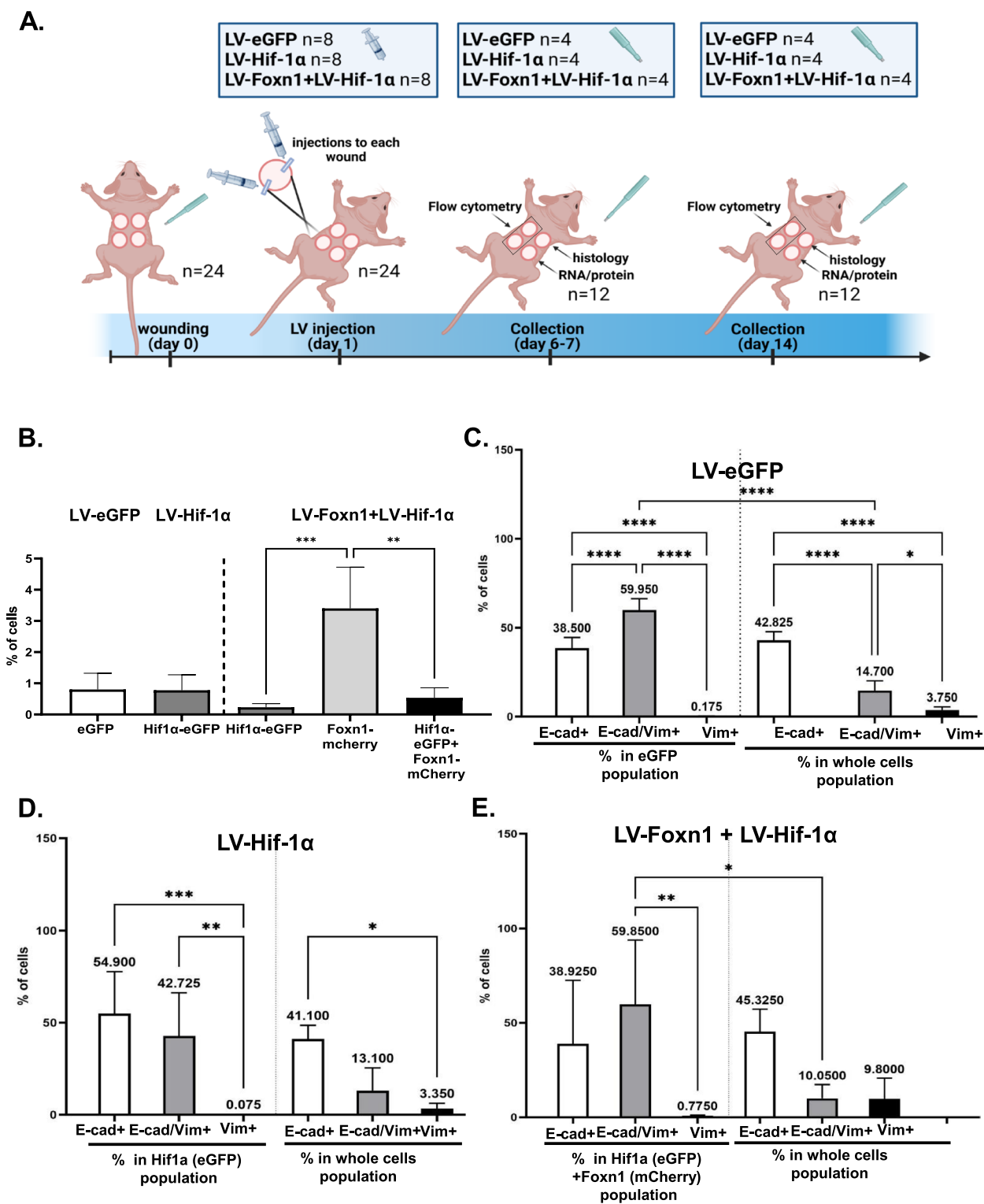
Fig. 7 (See legend on previous page.)

for mCherry signal in epidermis (arrowheads) and cells dispersed in dermal region of the skin (arrows) (Fig. 7F). Interestingly strong mCherry positivity was observed in the area of LV injection and newly formed tissues adjacent to wound margin (epidermis and dermis) but not in a distant wound bed region (Fig. 7F).

Macroscopic evaluation of skin wound healing in LV-treated Foxn1$^{-/-}$ mice

Next, we compared the size of the visible postwounded skin area among control (LV-eGFP), LV-Hif-1α- or LV-Hif-1α + LV-Foxn1-injected mice (Fig. 8). Macroscopic observations followed by measurements of the percentage of the initial (100%) postwounded surface area showed a significantly smaller and hardly visible postwounded area for control (LV-eGFP) mice at day 14 compared to that of the LV-Foxn1 + LV- Hif-1α-injected group ($p < 0.05$) (Fig. 8).

Foxn1/Hif-1α triggers distinctive ECM deposition in the wounded skin of Foxn1$^{-/-}$ mice

Hyaluronic acid

Our previous study showed that healed skin of Foxn1$^{-/-}$ mice is characterized by high levels of hyaluronic acid [2] which is consistent with another model of regenerative skin wound healing: mammalian foetuses [37]. To portray the differences in the resolution of skin wound healing between LV-eGFP-, LV-Hif-1α- or LV-Foxn1 + LV-Hif-1α-treated groups, we performed alcian blue staining of postwounded skin sections to visualize hyaluronic acid content (Fig. 9A). Blue deposits of staining product accumulated in wound beds, particularly under the new epidermis covering postwounded skin, which was detected at day 6 after injury (Fig. 9A). The wounded skin from the control mice (LV-eGFP-treated mice) showed the most intense signal and the largest alcian blue-stained area compared to that of the LV-Hif-1α- or LV-Foxn1 + LV-Hif-1α-treated groups (Fig. 9A).

Collagen

Next, to examine the potential related to Foxn1/Hif-1α changes in ECM, we stained histological sections of postinjured skin for collagen content (Masson trichrome staining, Fig. 9B). Blue-stained collagen fibres were deposited within the wounded skin area (day 14) of all examined groups regardless of treatment (LV-eGFP, LV-Hif-1α or LV-Foxn1 + LV-Hif-1α) (Fig. 9B). To further investigate the collagen content, we determined the collagen type I (*collagen 1a2*) and collagen type III
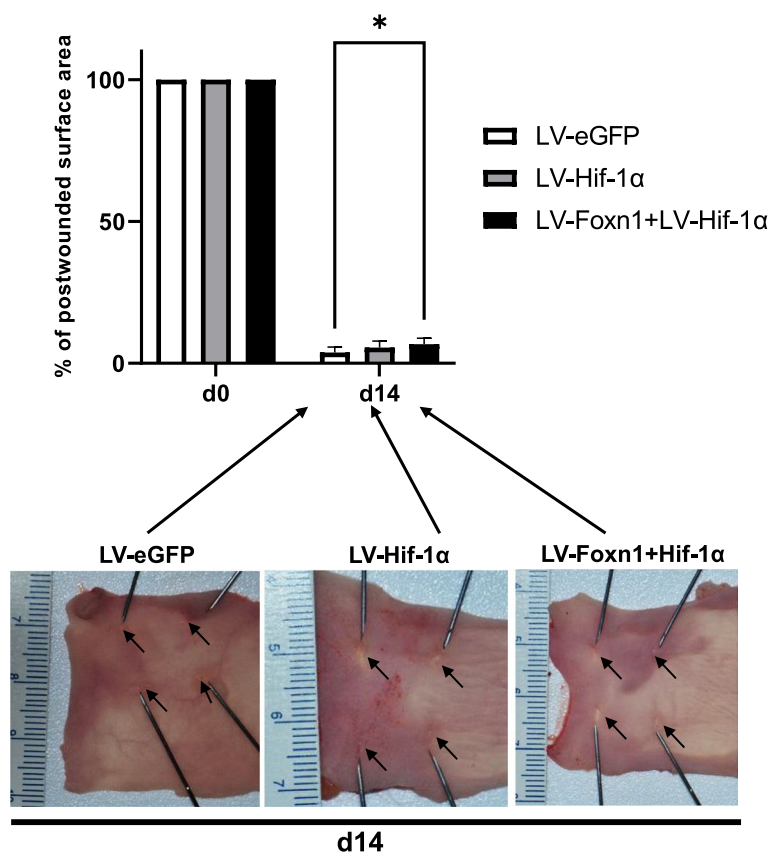
Fig. 8 LV-Foxn1 + LV-Hif-1α introduction into the postwounded skin (at day 1) of Foxn1$^{-/-}$ mice delays skin wound healing (at day 14). Morphometrical analysis of the percentage of the initial (100%; day 0) postwounded surface wound areas measured at postwounded day 14 (d14) ($n = 12$ measurements per time point). Values are the lsmean ± SE; asterisks indicate significant differences between the LV-eGFP- and LV-Hif-1α + LV-Foxn1-treated Foxn1.$^{-/-}$ mice at postwounding day 14 (*$p < 0.05$)
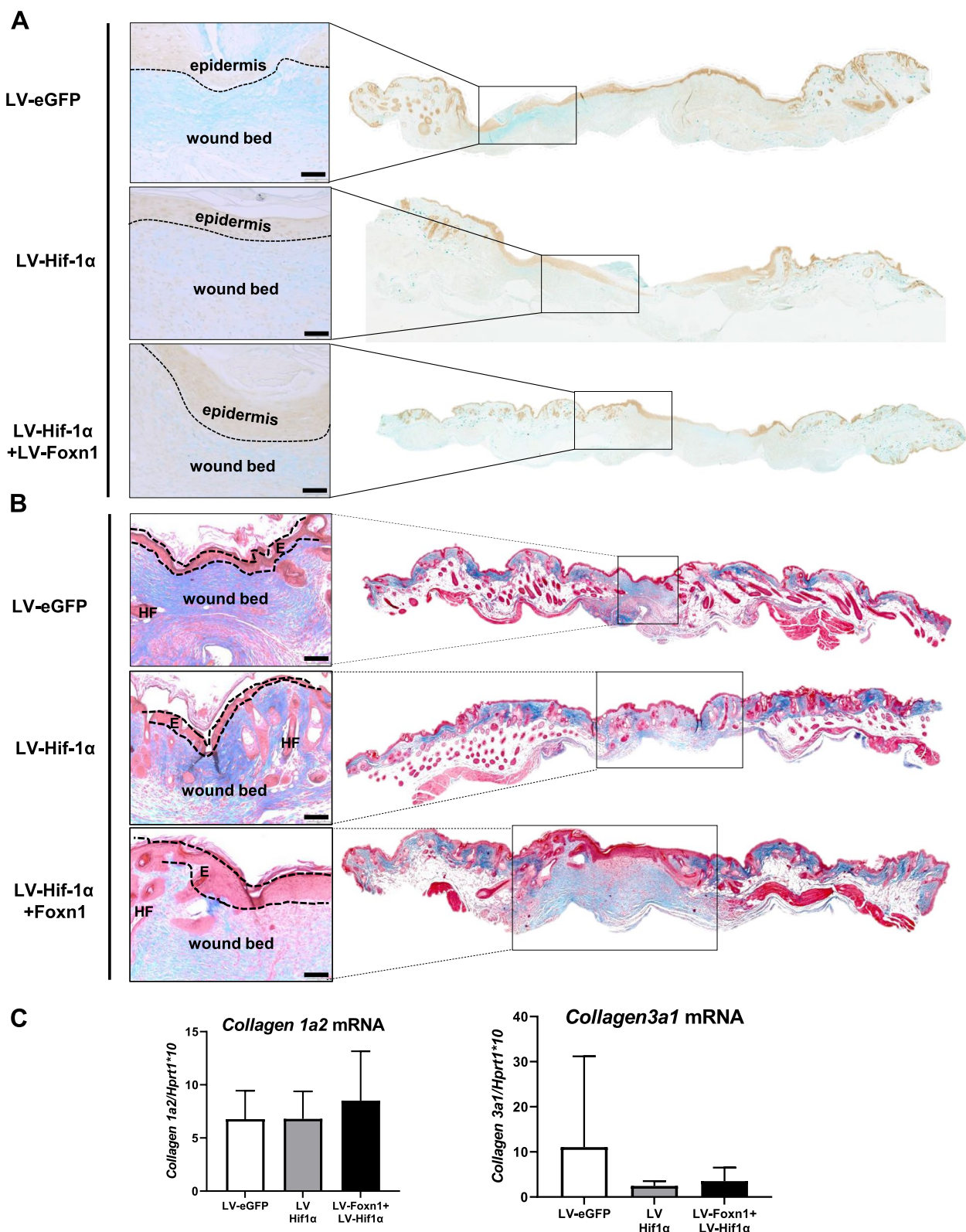
Fig. 9 Distinctive accumulation of hyaluronic acid (**A**) and collagen (**B**) and expression of *collagen 1a2* and *collagen 3a1* mRNA (**C**) in injured skin of LV-eGFP (control)-, LV-Hif-1α- or LV-Hif-1α + LV-Foxn1-treated Foxn1$^{-/-}$ mice at postwounding day 6 (**A**) and day 14 (**B,C**). **A** Representative histological sections stained with alcian blue (marker for hyaluronic acid) and immunostained for EpCAM (epithelial cell adhesion molecule; marker of epidermis) and **B** Masson trichrome (marker for collagen) collected from the skin of Foxn1$^{-/-}$ mice. Scale bar **A** 50 µm, **B** 100 µm

(*collagen 3a1*) mRNA expression in the wounded skin (Fig. 9C). No significant differences in collagen type I or collagen type III mRNA expression were detected among the examined groups (Fig. 9C), although collagen type III mRNA levels were elevated in the LV-eGFP-treated mice (control group) compared to the LV-Hif-1α- or LV-Foxn1 + LV-Hif-1α-treated mice (Fig. 9C).

For analysis of collagen type I vs. collagen type III content in situ, skin sections collected from LV-eGFP-, LV-Hif-1α- or LV-Foxn1 + LV-Hif-1α-treated mice on postwounding days 6 and 14 were stained with picrosirius red and analysed under polarized light microscopy [38] (Fig. 10). As shown in Fig. 10, the section background appears black, and the collagen bundles are red−yellow and green. A yellow−red colour of collagen staining represents collagen type I, whereas green-stained fibres represent collagen type III. The same settings and the same strategy of microscopic observations together with morphometric image analyses that allow qualitative and quantitative characterization of ECM collagen alterations for all specimens were applied. On postwounding day 6, high accumulation of collagen type III and low accumulation of collagen type I in the postwounding area were detected in all sections regardless of LV-eGFP, LV-Hif-1α or LV-Foxn1 + LV-Hif-1α incorporation (Fig. 10A–D). However, the detailed morphometric image analyses showed large differences related to the Foxn1, Hif-1α or eGFP (control) construct delivered to postinjured skin (Fig. 10D). The highest collagen type III content was detected in the control (LV-eGFP) mice (84.61%) in comparison to the LV-Hif-1α (43.94%; $p < 0.0001$) or LV-Foxn1 + LV-Hif-1α (58.94%; $p < 0.0001$)-treated mice (Fig. 10A–D). Interestingly, the LV-Hif-1α-treated mice, as the only mice among the experimental groups, showed a higher content of collagen type I (56.05%) vs. collagen type III (43.94%) in wounded skin at day 6. On day 14, collagen I (red−yellow colour of collagen bundles) represented the major type of collagen in postwounding skin sections regardless of LV-eGFP (72.12%), LV-Hif-1α (73.22%) or LV-Foxn1 + LV-Hif-1α (69.94%) treatment (Fig. 10E–I). However, the postwounded area at day 14 showed differences in collagen bundle arrangement among the experimental groups. Postwounded skin samples from the LV-Foxn1 + LV-Hif-1α or LV-Hif-1α treatment groups

revealed thick collagen fibres in parallel arrangement that are characteristic of scars (Fig. 10E−F). The control (LV-eGFP) mice displayed basket-weaved collagen bundles in the postwounding area that were similar to the structure of collagen observed in unwounded skin (compare Fig. 10G to Fig. 10H).

These data showing the decrease in collagen type III levels and hyaluronic acid content and the increase in postwounded skin area in Foxn1$^{-/-}$ mice due to LV-Hif-1α and LV-Foxn1 + LV-Hif-1α injection indicate that Hif-1α together with Foxn1 redirect the ECM organization from characteristic for scarless to scar-forming skin healing.

Foxn1 and Hif-1α cooperatively regulate ECM organization during the remodelling phase of skin wound healing

The apparent effect of LV-Hif-1α and LV-Foxn1 + LV-Hif-1α delivery into the wounded skin of regenerative Foxn1$^{-/-}$ mice (see Figs. 9 and 10) together with the results of proteomic analysis (Figs. 2 and 3) inspired us to analyse factors involved in ECM organization: Pai-1, Mmp9, Tgfβ1, Tgfβ3 and Vegfa protein levels in the wounded skin of LV-treated Foxn1$^{-/-}$ mice (Fig. 11, Additional file 2: Fig. S7, Fig. S8).

Pai-1 was assessed with Western blot followed by densitometric analyses, and we found nonsignificant differences in protein accumulation among postwounded skin of the LV-eGFP- (control), LV-Hif-1α- or LV-Foxn1 + LV-Hif-1α-treated mice. The lowest Pai-1 protein expression was detected in the LV-eGFP (control) mice, in which levels increased in the skin of the LV-Foxn1 + LV-Hif-1α mice and were the highest in the skin of the LV-Hif-1α-treated Foxn1$^{-/-}$ mice (Fig. 11A). Interestingly, Mmp-9 protein levels measured in the same postwounded skin samples showed inverse correlations (compare Fig. 11A to Fig. 11B). The highest levels of Mmp-9 protein were observed for the LV-eGFP mice (control), and the lowest were observed for the LV-Hif-1α-treated mice (Fig. 11B). The Tgfβ1, Tgfβ3 and Vegfa protein levels were similar among the treated groups (Fig. 11C–E). Although Tgfβ1 protein levels tended to increase in the skin of the LV-eGFP mice (control mice; Fig. 11C), Vegfa protein levels tended to decrease after LV-Foxn1 + LV-Hif-1α treatment (Fig. 11E).

(See figure on next page.)
Fig. 10 Evaluation of collagen type I vs. collagen type III content in stained picrosirius red histological skin sections collected from LV-eGFP (control)-, LV-Hif-1α- or LV-Hif-1α + LV-Foxn1-treated Foxn1$^{-/-}$ mice at day 6 (**A–D**) and day 14 (**E–G** and **I**) after injury. Representative histological sections of wounded (**A–C**; **E–G**; *n* = 3 per LV treatment) and unwounded skin (H; *n* = 3) were analysed. Collagen fibres: yellow−red (collagen type I) and green (collagen type III) were evaluated as a Relative Object Count [%] at postwounding days 6 (**D**) and 14 (**I**). Scale bar (A-G) 200 μm, insets (**A–G**) 50 μm and (**H**) 50 μm; wb – wound bed
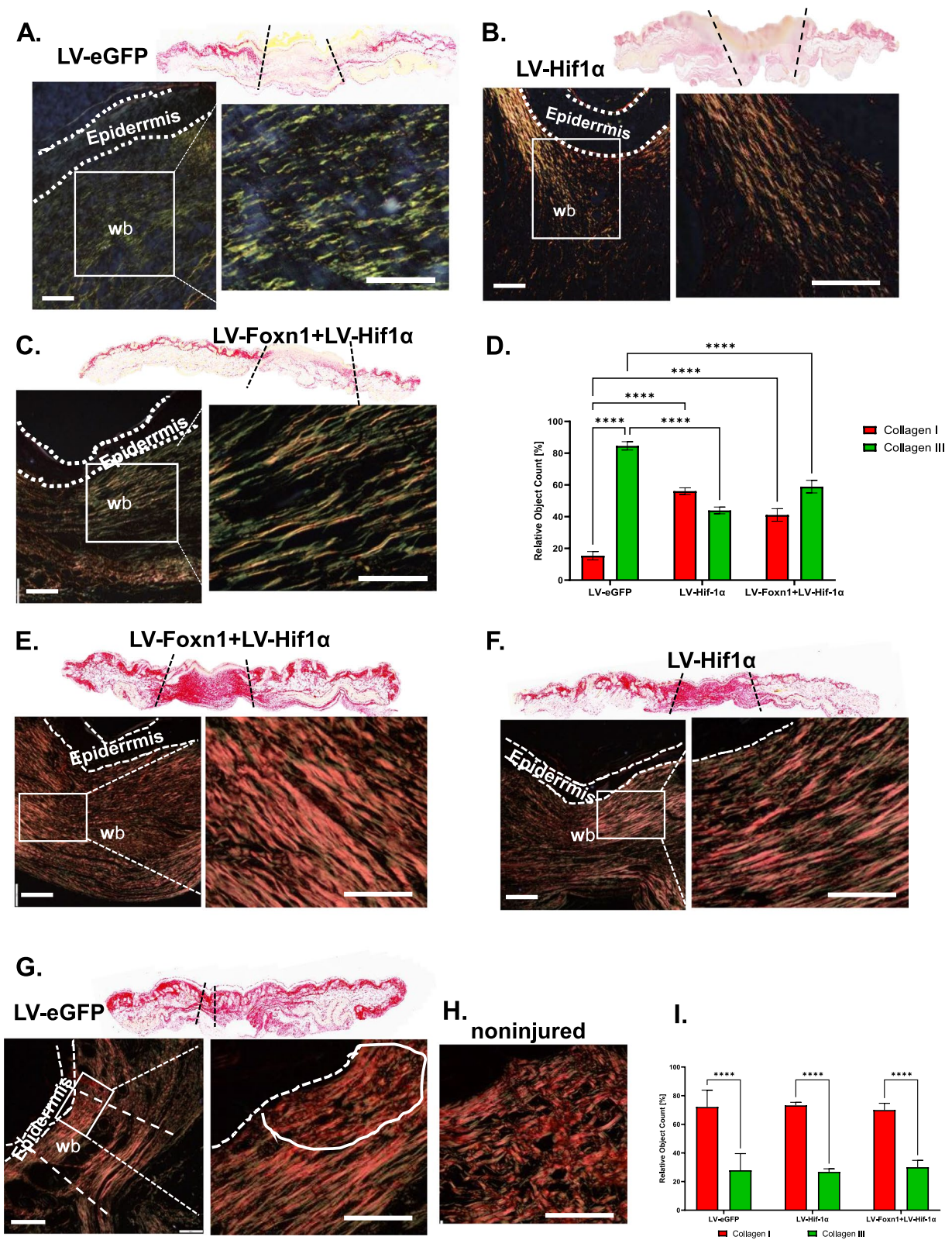
Fig. 10 (See legend on previous page.)
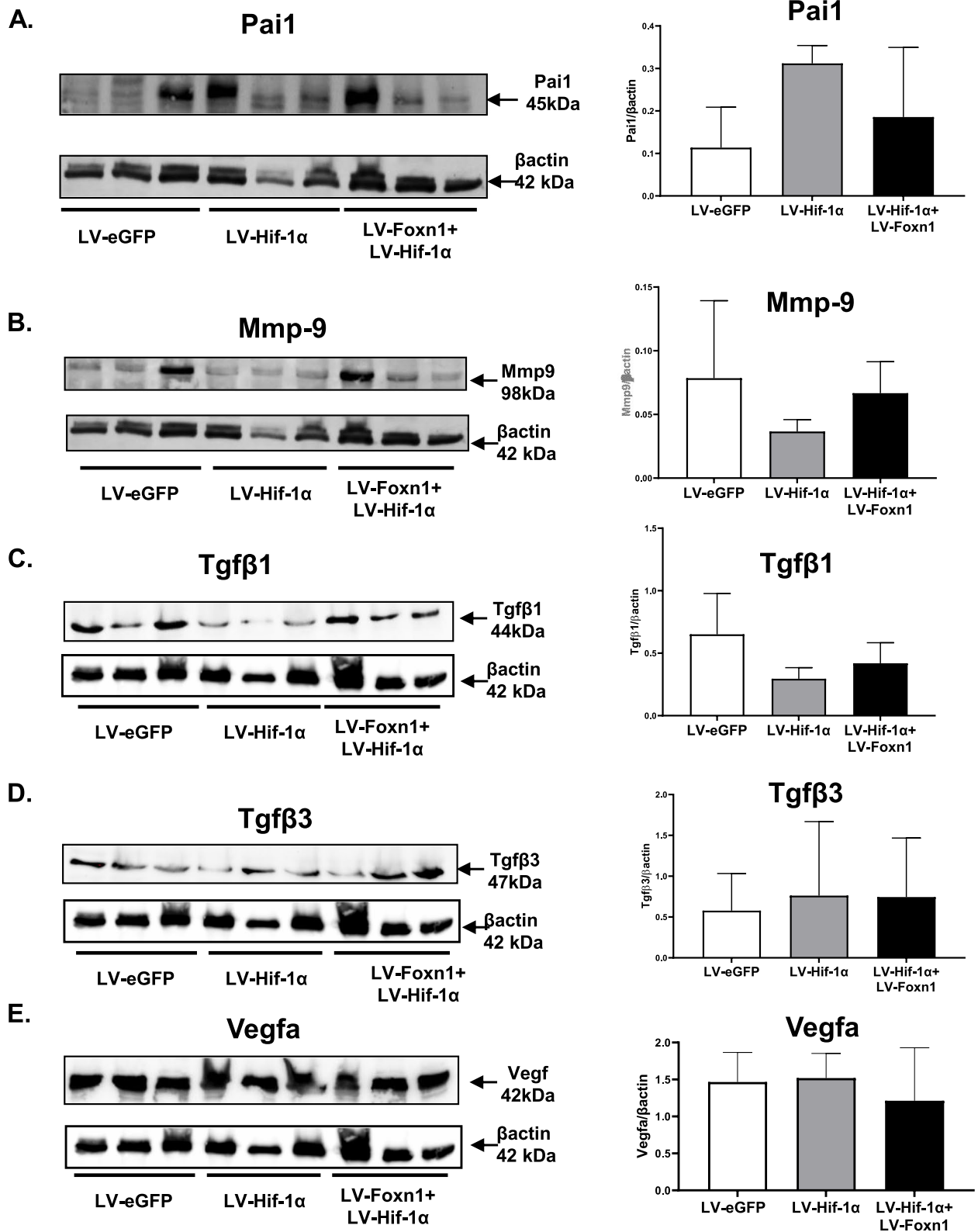
Fig. 11 LV-Hif-1α and LV-Foxn1 + LV-Hif-1α regulate ECM content in the wounded skin of Foxn1$^{-/-}$ mice. Western blot and densitometric analyses of Pai-1 (**A**), Mmp-9 (**B**), Tgfβ1 (**C**), Tgfβ3 (**D**) and Vegfa (**E**) proteins in the skin of LV-eGFP (control), LV-Hif-1α- or LV-Foxn1 + LV-Hif-1α-treated Foxn1.$^{-/-}$ mice at postwounding day 14 (*n* = 3 per treatment group)

Detected differences in Pai-1 protein levels related to LV-eGFP, LV-Hif-1α or LV-Foxn1 + LV-Hif-1α transfer into the wounded skin of regenerative Foxn1$^{-/-}$ mice (see Fig. 11A), prompted us to examine Pai-1 levels in the skin of Foxn1$^{+/+}$ and Foxn1$^{-/-}$ mice (Fig. 12A-B, Additional file 2: Fig. S9). Generally, accumulation of Pai-1 protein in intact and wounded skin was higher in the skin of Foxn1$^{+/+}$ than Foxn1$^{-/-}$ mice. Observed higher levels of Pai-1 in intact skin of Foxn1$^{+/+}$ mice (day 0) was further triggered by injury to reach statistical significantly ($p < 0.05$) increase in comparison to Foxn1$^{-/-}$ mice (day 1; Fig. 12A,B). The enlarged accumulation of Pai-1 corresponds with detected increase in Foxn1 protein at day 1 after injury in Foxn1$^{+/+}$ mice (Fig. 12C, Additional file 2: Fig. S10). Considering that our previous study showed triggered by wounding induction of Hif-1α primarily in the skin of Foxn1$^{+/+}$ mice [4], the findings collectively support a functional role for Foxn1/Hif-1α signalling in postwounded skin healing (Fig. 13).

Discussion

In the present study, we sought to determine/delineate the crosstalk between Foxn1 and Hif-1α signalling in the switch from regenerative to reparative skin wound healing in Foxn1$^{-/-}$ mice. First, using a proteomics approach, we showed that regenerative DFs (Foxn1$^{-/-}$) upon hypoxia and Foxn1 stimulation (Ad-Foxn1 transduction into keratinocytes in a coculture model) modify the levels and pattern of synthetized/released proteins, particularly those related to the ECM. Next, we demonstrated that the introduction of Foxn1 and Hif-1α via lentiviral injection into the wounded skin of regenerative Foxn1$^{-/-}$ mice activated reparative/scar-forming healing by increasing the wounded skin area and decreasing hyaluronic acid deposition and the collagen type III to I ratio. We found that the Pai-1 protein was stimulated by hypoxic conditions in regenerative Foxn1$^{-/-}$ DFs but was released by DFs to the culture media exclusively upon hypoxia and Foxn1 stimulation. We also showed: (i) higher levels of Pai-1 protein in Foxn1$^{+/+}$ DFs (scar-forming) than in Foxn1$^{-/-}$ DFs (scarless); (ii) a stimulatory effect of LV-Foxn1/LV-Hif-1α injection into the wounded skin of Foxn1$^{-/-}$ mice on Pai-1 protein levels, and (iii) triggered by injury increase in Foxn1 and Pai-1 protein in the skin of mice with active Foxn1 (Foxn1$^{+/+}$ mice).

Our previous studies, revealed that Foxn1 stimulates reparative (scar-forming) skin wound healing contributing to re-epithelialization, EMT and dWAT modification, acting as a regulator of Hif-1α and Fih1 activity [4, 8–11, 18].

We also showed that postwounded skin of Foxn1$^{-/-}$ mice (model of regenerative skin wound healing), in contrast to Foxn1$^{+/+}$ (model of reparative/scar forming skin wound healing), contained high and sustained levels of hyaluronic acid content, lower levels of hydroxyproline content and different collagen deposition [3, 4].
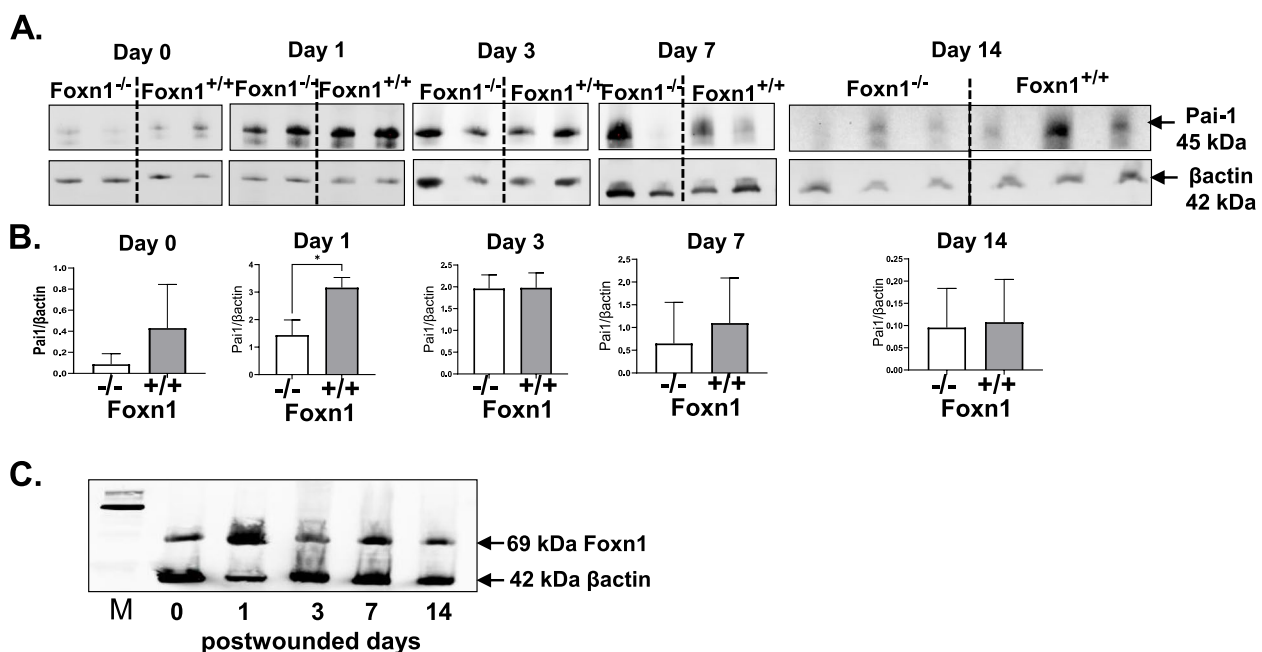
Fig. 12 Pai-1 (**A,B**) and Foxn1 (**C**) protein levels in the intact (day 0) and wounded (days 1, 3, 7, 14) skin of Foxn1$^{-/-}$ (**A,B**) and Foxn1.$^{+/+}$ (**A–C**) mice. Western blots (**A**, **C**) followed by densitometric analyses (**B**). Values are the lsmean ± SE; asterisks indicate significant differences (*$p < 0.05$)
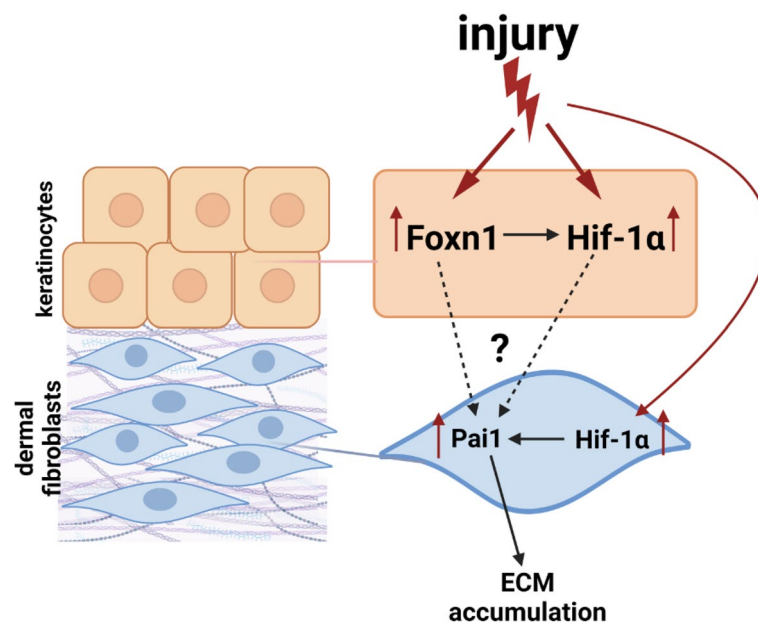
Fig. 13 Scheme of the proposed Foxn1 → Hif-1α → Pai-1 pathway in reparative scar-forming skin wound healing in Foxn1$^{+/+}$ mice

The present study examined whether Foxn1 introduced to the postinjured skin of Foxn1$^{-/-}$ mice may switch the regenerative to reparative skin wound healing process and revealed that Foxn1 together with Hif-1α modulates the postinjured skin of Foxn1$^{-/-}$ mice towards scar-forming characteristics. The effectiveness of intradermal injection of LV-Foxn1 and LV-Hif-1α into postwounded mouse skin was detected in our previous study [11]. LV-Foxn1 and LV-Hif-1α transduced into the skin of Foxn1$^{-/-}$ mice cooperatively regulated dWAT during the proliferative phase of skin wound healing through the Igf2 signalling pathway and reduced the macrophages content in the wound site [11]. Present study demonstrated that Hif-1α and Foxn1 introduced by LV to postwounded skin of regenerative Foxn1$^{-/-}$ mice promotes reparative/scar forming wound healing. Comparable approach although in promoting regenerative vs reparative skin wound healing was undertaken by Caskey et al. [39]. Lenti-HAS-1(hyaluronic acid synthase-1)-treated wounds of C57BL/6 mice demonstrated an increase in hyaluronic acid levels that is characteristic for regenerative foetal skin healing wounds [39]. The successful over-expression of HAS-1 in the wounds of lentiviral-HAS-1-treated mice was assessed by GFP expression (fluorescent stereomicroscopy) and by PCR assays. In our study efficacious Foxn1 and Hif-1α delivery into postwounded skin was evaluated by flow cytometry and histochemistry. The skin of Foxn1$^{-/-}$ mice treated with both LV-Hif-1α and LV-Foxn1 showed the highest percentage of transduced cells that confined the populations

of E-cadherin/Vimentin double positive and E-cadherin positive cells. The increase in the percentage of double positive cells for E-cadherin as epithelial marker and vimentin as marker of DFs supports detected in our previous study involvement of Foxn1 in EMT during skin wound healing [8, 9]. LV-mediated cutaneous gene transfer was exploited in in vitro, ex vivo and in vivo methodologies [38–44]. Efficiency of lentiviral gene transduction into keratinocytes was markedly enhanced with polybrene [44] the compound which was also applied in our in vitro experiments (see Fig. 6). The specificity of intradermal LV gene transfer was analysed on grafted human-on mouse skin model [42]. Intradermal injection of human skin showed stable and efficient gene transfer to human epidermal cells in the uppermost granular and cornified layers of epidermis or in all layers of epidermis when LV vector included WPRE (post-transcriptional regulatory element from woodchuck hepatitis virus) element. The intradermal gene transfer to human skin in a xenotransplanted mouse model showed efficacy and extensive transduction by lentiviral vector by monitoring bioluminescence signals [45]. The immunohistochemical approach to detect GFP expression revealed that intradermal injection of lentiviral vectors into human foreskin grafted onto immunocompromised mice transduced differentiated suprabasal keratinocytes and dermal fibroblasts [40]. In our study, immunohistochemical detection of mCherry positivity (LV-Foxn1-mCherry intradermal injection) was localized to epidermis and some dermal cells (see Fig. 7F). Yet, detected in our study: (i) an

increase in the wounded skin area, (ii) decrease in hyaluronic acid deposition,(iii) the collagen type III to I ratio observed in LV-Foxn1/LV-Hif-1α but not in control LV-GFP-treated postwounded skin of Foxn1$^{-/-}$ mice, provide data of successful and efficient gene transfer.

Hypoxia and hypoxia-associated factors (Hif-1α and Fih1) are important in directing skin wound healing: reparative, regenerative or impaired in diabetic wounds [13, 17, 46]. Botusan et al. showed that adenovirus-transferred stable forms of HIF-1α into wounded skin edges of diabetic mice improved skin healing [46]. HIF-1α transfer induced genes critical in cell motility (HSP-90) and angiogenesis (VEGF-A) which corresponded with histologically detected skin wound healing improvement [46]. Dysregulation in skin wound healing can also cause fibrotic disorders which manifest with abnormal accumulation of ECM components to form hypertrophic scars. The experiments performed on equine dermal fibroblasts revealed that hypoxia via HIF1α regulates ECM remodelling favouring ECM accumulation through increase in collagen (COL1A1) and decrease in MMP levels (MMP2) [47].

Although the phenomena of regenerative skin wound healing are incompletely understood, they have been associated with high levels of hyaluronic acid, a higher ratio of collagen type III to I, and modifications in MMPs/TIMPs and TGFβ1/3 in postwounded skin of regenerative models: mammalian foetuses and Foxn1$^{-/-}$ mice [2–4, 33]. In the present study, we showed that high levels of hyaluronic acid content and an increase in the collagen type III in the skin is lowered due to LV- Foxn1/LV-Hif-1α injections into postwounded skin of regenerative mice (Foxn1$^{-/-}$). At postwounding day 14, high levels of collagen type I and low levels of collagen type III were characteristic of all cohorts of mice regardless of LV treatment. However, exclusively postwounded skin of control (LV-eGFP) Foxn1$^{-/-}$ mice at day 14 displayed collagenous fibre arrangement characteristic of noninjured skin [48]. The remodelling of postwounded ECM is an important aspect of skin wound healing that may restore the characteristics of noninjured skin (regeneration) or form a collagenous scar (reparation). This process involves MMPs/TIMPs, components of the plasminogen activation system and Adamts [48] together with lysyl oxidase (LOX) and lysyl hydroxylases, which determine the extent of intermolecular crosslinking between collagens and elastin [49]. Our proteomics analyses revealed that Foxn1 and hypoxia regulate Foxn1$^{-/-}$ DFs and Foxn1$^{-/-}$ DFCM proteins involved in ECM organization: MMP-3, MMP-8, MMP-15 Adamts1, Adamts-5, Lox, Loxl2 and Pai-1. Subsequent experiments showed a stimulatory effect of LV-Hif-1α and LV-Foxn1 + LV-Hif-1α injected into postinjured skin of Foxn1$^{-/-}$ mice on Pai-1 protein

levels that accompanied the decrease in Mmp-9 protein levels found in the same tissues.

Pai-1, which is encoded by Serpin family E member 1 (SERPINE1), is a serine proteinase inhibitor that is a multipotent factor that participates in each stage of wound healing by modulating coagulation and inflammatory pathways, cell migration, tissue remodelling and fibrosis [50]. Pai-1 is a component of the plasminogen activation system that acts as an inhibitor of tissue-type plasminogen activator (tPA) and urokinase-type plasminogen activator (uPA). In the skin, Pai-1 is synthetized by keratinocytes, local inflammatory cells and DFs to regulate cell migration and is secreted into the ECM, where it plays an important role in the regulation of remodelling/degradation during skin wound healing. Elevated levels of Pai-1 have been associated with increased fibrosis in injured skin and tendons and in lung fibrosis and liver cirrhosis [51–53].

Interestingly, intact skin at E14 (regenerative mouse embryo at 14 days of development) showed much lower levels of Pai-1 than that at E18 (reparative). The differences were even stronger in wounded skin. Whereas postwounded skin of E14 showed a minimal increase in Pai-1, a significant and sustained increase was detected in E18 mouse skin [54]. Moreover, higher levels of Pai-1 were detected in postnatal mouse DFs than in foetal mouse DFs [55]. Our study harmonizes and supports observations showing that regenerative DFs (Foxn1$^{-/-}$), similar to foetal DFs and E14 skin, contained significantly lower levels of Pai-1 than reparative DFs (Foxn1$^{+/+}$) or E18 or postnatal DFs [54]. We also showed the stimulatory effect of Tgfβ1 or even stronger effect of Tgfβ3 on Pai-1 regulation, confirming that Pai-1 is a critical component of the Tgf-β-mediated tissue remodelling programme [56]. The proteomic analysis revealed that hypoxic conditions upregulate Pai-1 expression in DFs regardless of Ad-Foxn1 or Ad-GFP keratinocyte coculture, although exclusively upon coculture with Ad-Foxn1-keratinocytes, DFs release Pai-1 to the media. Furthermore, we identified Foxn1 and Hif-1α injected into the wounded skin of Foxn1$^{-/-}$ mice as transcription factors that upregulate Pai-1 expression during skin wound healing, suggesting the pathway of choice between regenerative and reparative healing. This finding was confirmed by detected increase in Foxn1 protein levels in postwounded skin of Foxn1$^{+/+}$ mice which correspond with enlarged Pai-1 accumulation (see Fig. 12). Collectively, these data support postulated involvement of Foxn1 and Hif-1α in the activation of Pai-1 during skin wound healing process. Intriguingly, the proteomic analysis also showed extremely high levels of very low-density lipoprotein receptor (Vldlr) protein in DFs upon hypoxia and coculture with Ad-Foxn1-transduced keratinocytes

Gawronska-Kozak *et al. BMC Biology*   (2024) 22:193

Page 20 of 28

(see Fig. 2D). Whether Vldlr may activate Pai-1 expression in DFs through binding vldl, as was shown for endothelial cells, merits further examination [57].

To understand the molecular basis of regenerative skin healing, Rinkevich et al. revealed the presence of two populations of DFs in the dorsal skin of mice: EPFs (Engrailed-1-lineage-positive fibroblasts) and ENFs (En1-linage negative fibroblasts), which are established embryonically [23]. During skin wound healing, EPFs appear to be a major mediator or fibrotic/scar outcome healing, whereas ENFs are associated with the embryonic dermis [22]. These researchers also showed that the ratio between ENFs to EPFs changes dynamically, particularly during embryonic development, towards an increase in the percentage of EPFs at the expense of ENFs [23] which corroborates the switch between regenerative vs. reparative (adult) skin wound healing in utero.

In our approach to disseminating/understanding the paradigm of regenerative vs. reparative injured skin healing, we have used different strategies in this study to reveal if and how the transcription factor Foxn1 expressed in keratinocytes may regulate not only keratinocytes but also underlying DFs. The initial study focused on the comparison of the transcriptomic profile of adult skin from Foxn1$^{-/-}$ mice (regenerative) to establish a model of regeneration of the skin of embryos at the period of regenerative competence (E14) to contrast it to the transcriptome of adult skin and the skin of embryos that passed the period of regeneration (E18) [58]. The data showed the resemblance of gene expression profiles that were shared by two models of skin regeneration: nude mice (Foxn1$^{-/-}$) and E14 foetuses (Foxn1$^{-/-}$) as consequences of Foxn1 deficiency. *Wnt*, *Bmp* and *Notch* signalling genes, among others, are affected by Foxn1 deficiency, including the Notch ligands *Dll1*, *Dll4* and *Dlk1* and the Bmp family members *Bmp2* and *Bmp4*, which are downregulated in the skin of Foxn1$^{-/-}$ mice [58]. These data are consistent with data by Driskell et al., showing that the increase/accumulation of Dlk1-positive fibroblasts results in skin scar-present healing [19]. Moreover, different regulation of Wnt family genes, such as upregulation of *Wisp2*, *Wnt10a*, *Wnt11*, *β-catenin*, the Wnt receptor frizzled 1 (*Fzd1* and *Fzd6*) along with downregulated Wnt pathway inhibitors, dickkopf 1 (*Dkk1*), frizzled-related protein (*Frzb*) and secreted frizzled-related protein 2 (*Sfrp2*), in Foxn1$^{-/-}$ skin may suggest, as proposed by Lee et al., that different branches of Wnt signalling differently participate in scarless versus scar-forming healing [59]. Furthermore, our transcriptomic [58] and present data together with the established role of Foxn1 in hair development [60] and the detected initial expression of Foxn1 in the skin at E16.5 support the hypothesis proposed by Lee et al. [59] which states

that the mechanisms that control embryonic hair follicle formation might function to control wound healing, since the transition from scarless to scar-forming pattern of repair during development coincides with hair follicle formation.

The Hippo pathway together with its downstream effectors Yes-associated protein (YAP) and TAZ has also been shown to regulate organ growth, regeneration and tissue repair [61, 62]. In the skin, YAP is localized to the epidermis and dermis, where it controls skin homeostasis and regulates the proliferation of keratinocytes and wound closure in mice [61, 63, 64]. A study by Mescharak et al. reported that blocking YAP signalling blocks En1 activation and prevents the conversion of ENFs (En-1-negative fibroblasts – regenerative) to EPFs (En-1-negative fibroblasts – regenerative), resulting in regenerative skin wound healing in a mouse model [27]. Subsequent studies showed that YAP inhibition activates the Wnt pathway regulator *Trps1*, which is involved in HF morphogenesis [28].

Our recent study analysing the effect of Foxn1 and hypoxia/normoxia on the proteomic signature of keratinocytes revealed that Ad-Foxn1 transduction into keratinocytes regardless of hypoxia or normoxia significantly upregulates YAP protein expression [18] which may support observations by others of cooperation of YAP/TAZ with other transcription factors [62]. Several data showed that YAP regulates Pai-1 [65, 66]. The synergistic effect of YAP and TGFβ on Serpine 1/Pai-1 induction was presented in lung cancer cells [56]. Whether the stimulatory effect of Foxn1 on YAP protein levels in keratinocytes upregulates Pai-1 in DFs to stimulate fibrotic skin wound healing in Foxn1$^{-/-}$ mice warrants future study.

Conclusions

The present data highlight that the interaction between Foxn1 and Hif-1α during cutaneous wound healing drives the physiological decision between regeneration (Foxn1$^{-/-}$; scarless healing) or repair (Foxn1$^{+/+}$; scarring). We showed that hypoxia and Foxn1 modify the protein profile and functionality of regenerative Foxn1$^{-/-}$ DFs, particularly within the plasminogen activating cascade. We identified Pai-1 (an element of the plasminogen activating cascade pathway) as a possible molecular target to stimulate scarring. We also found higher levels of Pai-1 protein in Foxn1$^{+/+}$ DFs (reparative/scar-forming) than in Foxn1$^{-/-}$ DFs (regenerative/scar-less) and that triggered by injury the increase in Foxn1 is accompanied by the increase in Pai-1 protein in Foxn1$^{+/+}$ mice. Furthermore, we demonstrated that the introduction of Foxn1 and Hif-1α into the wounded skin of regenerative Foxn1$^{-/-}$ mice activates reparative/scar-forming healing.

Our study on transcription factors, the Foxn1 and Hif-1α signalling pathways, that affect skin wound healing fits in the proposed scenario of Wnt and Hippo signalling regulating the decision between regenerative vs. reparative skin wound healing.

Methods

Animals

The in vivo studies were performed on 7–16-week-old female Foxn1$^{-/-}$ (CBy.Cg-Foxn1/cmdb, $n=36$) that were housed in individually ventilated cages (IVCs) in a temperature (22 °C) and humidity (55%)-controlled room with a 12-h light/12-hdark cycle at the Center of Experimental Medicine (CEM), Medical University of Bialystok, Poland.

The in vitro studies were performed on keratinocytes isolated from newborn Foxn1$^{+/+}$ (C57BL/6) mice, DFs isolated from 4- to 10-month-old: C57BL/6 mice (DFs Foxn1$^{+/+}$) or CBy.Cg-Foxn1/cmdb mice (DFs Foxn1$^{-/-}$). C57BL/6 mice were bred and housed in a temperature- and humidity-controlled room (22 ± 2 °C and 35–65% humidity) with a 12-h light/12-h dark cycle at the Institute of Animal Reproduction and Food Research, Polish Academy of Sciences, Olsztyn, Poland.

The experimental animal procedures were approved by the Ethics Committee of the University of Warmia and Mazury (Olsztyn, Poland), No. 68/2018. The study was carried out in accordance with EU Directive 2010/63/EU of the European Parliament and of the Council on the Protection of Animals Used for Scientific Purposes (OJEU, 2010. Official Journal of the European Union. Directive 2010/63/EU of the European Parliament and of the Council on the protection of animals used for scientific purposes. OJEU. [cited 2010 Oct 20]; Series L 276:33–79).

Cell isolation and culture

DFs and keratinocytes were isolated and cultured as described before [18].

Briefly, DFs were isolated from the excised skin of Foxn1$^{-/-}$ mice that were subjected to enzymatic digestion in collagenase type I (3.68 mg/ml; Sigma-Aldrich Co.) for 80 min at 37 °C in an incubator shaker and filtered (100-μm strainers). The cells were centrifuged for 5 min at 1200 rpm at room temperature. The pelleted cells were suspended and plated ($p=0$) in 60-mm Petri dishes in DMEM/F-12 medium (Sigma-Aldrich Co.) with 15% foetal bovine serum (FBS, Life Technologies, Thermo Fisher Scientific) and 1% gentamicin/amphotericin (Life Technologies, Thermo Fisher Scientific). Confluent DFs were trypsinized (0.05%; Sigma-Aldrich Co.) and frozen for further experiments.

Keratinocytes were isolated from the skin of newborn Foxn1$^{+/+}$ (C57BL/6) mice as described before [4, 18]. Collected skin samples were incubated in dispase (6 U/mL; Life Technologies) overnight at 4 °C to separate epidermis from dermis. The next day, separated epidermis was digested in 0.05% trypsin–EDTA (Life Technologies) for 3 min and filtered through a 70-μm strainer (Falcon, A Corning Brand, NY, USA) for keratinocyte isolation. Keratinocytes were collected by a series of three rounds of trypsin digestion (at 37 °C) and filtration followed by centrifugation at $300\times g$ for 9 min at room temperature. The pelleted cells were suspended and seeded ($p=0$) in inserts (CorningR BioCoat™ Control Inserts with 0.4 μm PET Membrane) in Dulbecco's modified Eagle's medium (DMEM/F-12; Sigma-Aldrich Co.) supplemented with 10% foetal bovine serum (FBS; Life Technologies), 0.2% Primocin (InvivoGen) and 120 μM β-mercaptoethanol (Sigma-Aldrich). After 24 h, the media were exchanged to CnT medium (CELLnTEC).

Keratinocytes-DFs co-culture for proteomics experiments

The co-culture model was described before [18]. Briefly, freshly isolated keratinocytes from the skin of newborn Foxn1$^{+/+}$ mice were seeded at densities of 1.3×10^6 were cultured in inserts (CorningR BioCoat™ Control Inserts with 0.4 μm PET Membrane). After reaching 70% confluency, keratinocytes were transduced with Foxn1-GFP-expressing (Ad-Foxn1) or control (Ad-GFP) adenoviruses as described before [4, 18]. DFs ($p=1$) were seeded in 6-well plates (Corning Falcon) at a density of 0.3×10^6 cells per well. For co-culture experiments, keratinocytes (cultured in inserts) and transduced with Ad-Foxn1 or Ad-GFP adenoviruses were set up with DFs (cultured on the bottoms of 6-well plates) and cultured under normoxic (21% O_2) or hypoxic (1% O_2) conditions for 24 h.

DFs collection and preparation for proteomics analyses

DFs, cultured on the bottom of the 6-well plates, after 24 h of co-culture with keratinocytes under normoxic or hypoxic conditions ($n=3$, total $n=6$ animals) were washed with cold PBS. Then, lysis buffer (2% SDS, 50 mM Tris–HCl pH 7.55; Sigma-Aldrich Co.) with protease inhibitor cocktail (Sigma-Aldrich Co.) was added, and the cells were incubated for 10 min on ice. DFs were scraped off from the dish with a plastic cell scraper, and suspension was transferred into a precooled microcentrifuge tube for further sonication (3×20 s, 20 kHz; with Vibra-Cell VCX 130 PB sonicator). The cell lysates were incubated for 45 min on ice and centrifuged at 10,000 g for 15 min at 4 °C. The supernatant was transferred to new tubes, and the protein concentrations were measured using the standard Bradford protocol (Bradford

Gawronska-Kozak *et al. BMC Biology*   (2024) 22:193

Page 22 of 28

Reagent, Sigma-Aldrich Co.). Cell lysates were stored frozen at -80 °C for further experiments.

DFCM collection and preparation for proteomics analyses

Conditioned medium (DFCM) collected from DFs co-cultured with keratinocytes (transduced with Ad-Foxn1 or Ad-GFP) for 24 h under normoxic and hypoxic conditions was centrifuged at 300 *g* for 10 min at 4 °C, filtered, and stored frozen at -80 °C for further analysis.

Frozen DFCMs were transferred to a Falcon tube with 2% sodium deoxycholate solution (v/v) (Thermo Fisher Scientific) and incubated on ice for 30 min. After incubation, trichloroacetic acid (Sigma-Aldrich Co.) was added to each tube to a final concentration of 7.5% (v/v) and incubated again on ice for 60 min. Precipitated proteins were collected by centrifugation at 15,000 *g* for 20 min at 4 °C, and the supernatants were discarded. Then, 20 ml of 100% ice-cold (-20 °C) acetone was added, and the pellets were vortexed until the precipitate was dissolved, followed by 10 min incubation at -20 °C. After centrifugation the wash of the protein pellets was repeated twice as described before [18]. The pellets were air-dried and dissolved in 2% SDS and 50 mM Tris–HCl (pH 7.55; Sigma-Aldrich Co.). The protein concentration was determined by the BCA method (Thermo Fisher Scientific).

S-TRAP

Proteins isolated from DFs and conditioned medium samples (DFCM) were thawed, and DNA was sheared by 5 min sonication with 30 s on/off cycles. Samples were clarified by centrifugation for 10 min at 16,000 *g*. All proteins from the conditioned medium samples (ranging from 8.6 to 20.8 μg of proteins in volume of ~ 100 μl) and 25 μg from cell lysate samples were taken for trypsin digestion with S-Trap micro columns (ProtiFi) as described before [18].

Before mass spectrometry (MS) analysis, the digested peptides were reconstituted to 0.1% formic acid, and peptide concentrations were determined with a NanoDrop One spectrophotometer (Thermo Scientific). For retention time calibration, peptide samples were spiked with iRT-peptides (Biognosys AG) at a ratio of 1:60 for DF samples and at a ratio of 1:40 for DFCM samples. For MS analysis, 400 ng of peptides from each conditioned media sample and 500 ng peptides of each cell lysate sample were used.

Protein analysis by LC–MS/MS

Relative protein quantitation was determined by the data-independent acquisition (DIA) MS method. The LC–MS/MS analyses were performed on a nanoflow HPLC system (Easy-nLC1200, Thermo Scientific) coupled to an Orbitrap Fusion Lumos mass spectrometer (Thermo Scientific) equipped with a nanoelectrospray ionization source. A detailed description of the procedure was presented before [18].

Gene ontology and bioinformatics analyses

Gene ontology (GO) and Kyoto Encyclopedia of Genes and Genomes (KEGG) annotation of differentiated proteins was performed by using online bioinformatics tool of PANTHER (Protein Analysis Through Evolutionary Relationships). Classification System, version 16.0 (released 2022–10; https://pantherdb.org/) [67]. The analysis of potential protein–protein interactions was performed with the Search Tool for the Retrieval of Interacting Genes (STRING) online database, version 11.0 (with a medium confidence score cutoff of 0.4) (https://string-db.org) [68].

Protein–protein interaction networks were constructed using Cytoscape software (Cytoscape.org), version 3.8.2. [69]. A heatmap containing differentially expressed proteins detected in DFs co-culture with keratinocytes transducted by Ad-Foxn1 or Ad-GFP under hypoxic or normoxic conditions was created using GraphPad Prism Version 9.0 (GraphPad Software, La Jolla, CA, USA).

DFs functionality analyses

MTT

DFs isolated from Foxn1$^{-/-}$ mice ($n=5$, each in triplicate) were seeded in 24-well plates ($p=1$) at a density of 0.05×10^6 cells/well and cultured in a 1:1 ratio with (i) conditioned medium (KCM) collected from keratinocytes transduced with Ad-Foxn1 or Ad-GFP and co-cultured with DFs for 24 h respectively under normoxic or hypoxic conditions and (ii) DMEM/F-12 medium with 15% FBS and penicillin/streptomycin for 24 h under hypoxic or normoxic conditions. To assess metabolic activity 10 μl of sterile MTT solution (3-[4,5-dimethyl-thiazol-2-yl]-2,5-diphenyltetrazolium bromide; 5 mg/ml; Sigma-Aldrich Co.) was added to each well and incubated for 4 h (normoxia or hypoxia). After incubation, the medium was removed, and formazan crystals were dissolved in 100 μl of DMSO within 30 min in an incubator (37 °C) with gentle shaking (30 rpm). Absorbance was measured at 570-nm using a microplate reader (Multiskan Sky Microplate Spectrophotometer, Thermo Fisher Scientific).

BrdU assay

DFs isolated from Foxn1$^{-/-}$ mice were seeded ($p=1$) in 6-well plates at a density of 0.3×10^6/well. After the cells reached 50% confluency, DFs were culture in a 1:1

Gawronska-Kozak *et al. BMC Biology* (2024) 22:193

Page 23 of 28

ratio with (i) conditioned medium (KCM) collected from keratinocytes transduced with Ad-Foxn1 or Ad-GFP and co-cultured with DFs for 24 h under normoxic or hypoxic conditions and (ii) DMEM/F-12 medium with 15% FBS and penicillin/streptomycin respectively under hypoxic or normoxic conditions. After 8 h of culture, 10 µl of BrdU (1 mM) was added to each well, and the cells were incubated for the next 16 h. Then, the cells were trypsinized (0.05% trypsin–EDTA; Life Technologies), suspended in Dulbecco's modified Eagle's medium (DMEM/F-12; Sigma-Aldrich Co.) with 15% foetal bovine serum (FBS; Life Technologies) and 1% antibiotics (penicillin/streptomycin, Sigma-Aldrich Co.) and counted in automatic counts (Countess II, Invitrogen by Thermo Fisher Scientific). Next, the cells were centrifuged at 1200 rpm for 5 min at RT and suspended in warm sterile PBS. The flow cytometry assay was performed according to the manufacturer's protocol [BD Pharmingen BrdU Flow Kit, Becton Dickinson Cat# 559,619 (FITC)]. The labeled cells were analysed using a BD LSRFortessa Cell Analyzer flow cytometer (Becton Dickinson) and BD FACSDiva v6.2 software (Becton Dickinson). The data are expressed as the percentage of BrdU-positive cells per gated cell.

Migration assay

DFs ($p = 1$) isolated from skin samples of 4–6-month-old Foxn1$^{-/-}$ (CBy. Cg-Foxn1 < nu >/cmdb) mice were seeded in 12-well plates at a density of 0.1×10^6 per well ($n = 4$; each in duplicate). For prevention of cell proliferation, DFs were incubated for 3 h with mitomycin C (10 µg/ml) in DMEM/F-12 medium containing 15% FBS and 1% antibiotics (penicillin/streptomycin, Sigma-Aldrich). The cell monolayers were wounded by scratching a straight line throughout the center of the entire 12-well plate with a 200-µl pipette tip. Debris was removed by washing the cells with PBS. Then, the cells were cultured in a 1:1 ratio with (i) conditioned medium (KCM) collected from keratinocytes transduced with Ad-Foxn1 or Ad-GFP and co-cultured with DFs for 24 h under normoxic or hypoxic conditions and (ii) DMEM/F-12 medium with 15% FBS and penicillin/streptomycin respectively under hypoxic or normoxic conditions. Images were captured with an Olympus microscope (IX51) equipped with an Olympus digital camera (XC50) and analysed with ImageJ (SciJava software, National Institutes of Health; NIH). Three representative images of scratched areas were photographed, and the distances between scratched edges were measured. The distance at 0 h was considered to be 100%. The scratched areas were monitored until closure (at 0, 3, 6, 20, 24, and 30 h time points).

Keratinocytes/DFs in vitro lentiviral (LV) transduction assay

Lentiviral Vector Construct was prepared at Virus Vector Core, Turku Centre for Biotechnology BioCity, Finland, as described before [11].

Briefly, lentiviral transfer vectors were prepared by cloning full-length Hif-1(NM_001313919) into pEZ-Lv215, to generate Hif-1-IRES-GFP, and full-length FOXn1 (NM_008238) into pEZ-Lv214, to produce FOXn1-IRES-Cherry (GeneCopoeia, Rockville, MD, USA). Lentivirus particles containing either transgenes or just eGFP (empty/control), were produced in the 293FT packaging cell line (high-glucose DMEM, 10% FBS, 0.1 mM NEAA, 1 mM MEM sodium pyruvate, 6 mM L-glutamine, 1% penicillin/streptomycin and 0.5 mg/mL geneticin) by transient cotransfection using the calcium–phosphate precipitation method as described before [70].

Keratinocytes and DFs were isolated from the skin of new born C57BL/6 mice as previously described [18]. Freshly isolated cells were seeded in 6-well plates at a density of 0.2×10^6 per well ($n = 3$) and incubated at 37 °C, 5% CO_2 till 70% of confluency. Monolayered cells (keratinocytes or DFs) were transduced with LV-Hif-1α or LV-Foxn1 particles applying three dilutions of 5 µl, 10 µl, or 15 µl for each LV in serum-free CellnTec (keratinocytes) or DMEM (DFs) media. To increase the efficiency of viral transduction, media were supplemented with polybrene (Sigma-Aldrich) at final concentration of 8 µg/ml. After 24 h post transduction, complete media (CellnTec with supplements for keratinocytes or DMEM/F12 with 15% FBS for DFs) were added to each well. Media were changed every 2 days of culture. The transduction efficiency was analysed 5 days post transduction by quantitative real-time PCR.

Wound model

At the time of wounding, animals were anesthetized with isoflurane, and a sterile 4-mm-diameter biopsy punch (Miltex GmbH, Rietheim-Weilheim, Germany) was used to create four excisional wounds on the backs of the mice. After wounding, mice were transferred to individual cages and observed until recovery. The following day (day 1), mice were anesthetized with isoflurane and lentivirus vectors (LVs): LV-Hif1a, LV-Foxn1 + LVHif1a, or LV-GFP (control) at a dose of 10^6 TU in a 50-µL volume were injected into the base and margin of each wound on the dorsal skin of the mice as described before [11]. Animals were sacrificed on days 6 and 14 ($n = 4$ animals/per vector/per day of wounding) and skin samples (8-mm diameter) were collected. Two 8-mm-diameter skin biopsy punches from each animal were frozen in liquid nitrogen for protein/RNA isolation or fixed in formalin for histological analysis. Next two skin biopsy punches were used for cell isolation followed by flow cytometry assay.

Gawronska-Kozak *et al. BMC Biology*   (2024) 22:193

Page 24 of 28

The mice and the wounded and LV-injected skin areas were observed every post-wounding day, with meticulous, detailed notes made by an unbiased experimenter. Body mass was measured every week through 4 weeks of experiment.

Western blot

Frozen skin samples collected at day 14 after injury were powdered in liquid nitrogen using a prechilled mortar and pestle, and then, homogenized in RIPA buffer containing protease inhibitor cocktail (Sigma-Aldrich), phosphatase inhibitor cocktail (Sigma-Aldrich), and phenylmethane-sulfonyl fluoride (PMSF, Sigma-Aldrich), followed by sonication (3×5 s) with a sonicator (Vibro-Cell VCX 130 PB). Total cell lysates (DFs) were prepared in 400 μl RIPA buffer containing the abovementioned inhibitors. Protein concentration was measured by Bradford protein assay (Sigma-Aldrich). Thirty micrograms of proteins was separated on 9% Tricine gels and transferred to polyvinylidene difluoride membranes (Merck Millipore). The membranes were incubated separately with anti-Mmp-9 (1:1000, Cat# AB19016, Merck Millipore), anti-Vegfa (1:200, Cat# 46,154, Abcam), anti-Pai1 (1:1000, Cat# ab182973, Abcam), anti-Tgfβ1 (1:500, Cat# ab179695), anti-Tgfβ3 (1:100, Cat# ab15537, Abcam), anti-Foxn1 (1:500, Cat# ab113235, Abcam) or anti-β-actin (1:1000, Cat# 8226, Abcam), followed by incubation with fluorescent secondary antibodies against Alexa Fluor 594 (1:1000, Cat#A11037, Invitrogen) or Alexa Fluor Plus 800 (1:1000, Cat#A32789, Invitrogen) for 1 h. Bands were visualized using the ChemiDoc Touch Imaging System (Bio-Rad Laboratories, Inc) and analysed using Image Lab Software (Bio-Rad Laboratories, Inc) according to the manufacturer's protocol.

Western Blot analyses for Pai-1 (Fig. 12A-B) and Foxn1 (Fig. 12C) were performed on skin samples collected during our previous experiments [4] using anti-Pai-1 (1:1000, Cat# ab182973, Abcam) or anti-Foxn1 (1:500, Cat#ab113235, Abcam) antibodies.

Histology

Formalin-fixed skin samples were processed, embedded in paraffin, and sectioned at 5 μm. Slides for selectively highlight collagen networks (collagen 1 and collagen 3) were stained with picrosirius red (Direct Red 80, Catalog# 36–554-8, Sigma-Aldrich Co.) for 1 h. After staining, sections were washed in two changes of acidified water (0.5% acetic acid) and dehydrated with three changes of 100% ethanol. The sections were visualized using (i) GRUNDIUM OCUS® microscope scanner, (ii) an Olympus microscope (BX43) with polarized light and photographed with an Olympus digital camera (XC50). Analysis of collagen fibres: yellow–red (collagen type I) and green (collagen type III) were performed [37] as

a Relative Object Count [%] with Olympus CellSens Dimension Software.

Slides for collagen detection were stained with Masson's Trichrome according to the manufacturer's instructions (Trichrome Stain Kit, Abcam).

Immunohistochemical procedures were performed on skin sections with antibody to EpCAM (1:400, cat# ab71916, Abcam) or mCherry (1:100, cat# ab167453, Abcam). Antibody binding was detected using the ABC complex (Vector Laboratories, Inc.). For mCherry detection assay, skin sections were counterstained with haematoxylin. Peroxidase activity was revealed using 3.3- diaminobenzidine (DAB; Sigma-Aldrich Co.) as a substrate. For hyaluronan determination, the EpCAM immunostained skin sections were washed with 3% acetic acid for 3 min and stained for 30 min with Alcian Blue 8 GX (AppliChem GmbH). After staining, sections were rinsed 3% acetic acid then washed with tap water and quickly dehydrated with two changes of ethanol. The sections were visualized using an Olympus microscope (BX43), photographed with an Olympus digital camera (XC50), and analysed with Olympus CellSens Software.

RNA isolation and quantitative RT-PCR

Total RNA extraction from skin samples was performed using TRI Reagent Solution (Thermo Fisher Scientific by Invitrogen) according to the manufacturer's instructions. Quantity and quality of RNA were confirmed on NanoDrop 1000 (Thermo Fisher Scientific) and through agarose gel electrophoresis. High-Capacity cDNA Reverse Transcription Kit with RNase Inhibitor (Applied Biosystems by Thermo Fisher Scientific) was used to synthesize cDNA from 500 ng of total RNA. To measure mRNA levels, Single Tube TaqMan® Gene Expression Assays (Life Technologies by Thermo Fisher Scientific) were used (*collagen 1a2*, cat# Mm 00483888_m1; *collagen 3a1*, cat# Mm01254476m1 and *Hprt-1*, cat# Mm01545399m1, *Foxn1*, cat# Mm01298129m1). Amplification was performed under the following conditions: initial denaturation for 10 min at 95 °C, 40 cycles of 15 s at 95 °C and 1 min at 60 °C in 7900HT Fast Real-Time PCR System. Each run included standard curve based on aliquots of pooled selected RNA samples. All samples were analysed in duplicates. mRNA expression levels were normalized to the housekeeping gene *Hprt-1* and multiplied by 10.

Flow cytometry analysis

Flow cytometry was performed according to the previously described protocol [11]. In brief, skin samples were collected from Foxn1$^{-/-}$ mice injected with LVs-empty (GFP), LV-Hif-1 α (eGFP) or LV-Foxn1 (mCherry)+LV-Hif-1α (eGFP) at post-wounded day 14. Tissue specimens were processed, as previously described [4]. Cells were stained with the following antibodies: anti-mCherry-Alexa Fluor

647 (Thermo Fisher Scientific, cat # M11241, Waltham, MA, U.S.A.); anti-GFP-Alexa Fluor 488 (Thermo Fisher Scientific; cat # A21311, Waltham, MA, U.S.A.); anti-E-cadherin-PE (BioLegend, cat # 147,304, San Diego, CA, U.S.A.); and anti-vimentin (Abcam, cat # ab92547, Cambridge, UK), conjugated with FITC (Lynx Rapid FITC Antibody Conjugation Kit, cat # LNK061F; Bio-Rad Laboratories, Inc., Berkeley, CA, U.S.A.) or PeCy7 (Lynx Rapid PECY7 Antibody Conjugation Kit, cat # LNK112PECY7). The labeled cells were washed in a perm/wash buffer (BD Biosciences, Franklin Lakes, NJ, U.S.A.) and fixed in a cytofix/cytoperm buffer (BD Biosciences, Franklin Lakes, NJ, U.S.A.). A BD LSR Fortessa Cell Analyzer flow cytometer (Becton Dickinson and Company, BD Biosciences, San Jose, CA, U.S.A.) and BD FACS Diva v6.2 Software (Becton Dickinson, Franklin Lakes, NJ, U.S.A.) were used. The total number of cells analysed for each sample was ~ 50,000.

Statistical analysis

Statistical analysis was performed with GraphPad Prism, Version 9.1.2 (GraphPad Software, La Jolla, CA, USA). All data were checked for normality using the Shapiro–Wilk test. One-way analysis of variance with post hoc Tukey's test or two-way analysis of variance was used. Data are expressed as the mean ± standard deviation (SD). A value of $p < 0.05$ was considered statistically significant; * $p < 0.05$, ** $p < 0.01$, *** $p < 0.001$ and **** $p < 0.0001$.

Availability of supporting data

The mass spectrometry data has been deposited to Proteomics Identifications Database (PRIDE) with the dataset identifier PXD041939 [36].

https://www.ebi.ac.uk/pride/archive/projects/PXD041939.

Abbreviations

Ad-Foxn1	Foxn1-eGFP-expressing adenovirus
Ad-GFP	GFP-expressing control adenovirus
AP-1	Activator protein 1
BMP2	Bone Morphogenetic Protein 2
BrdU	Bromodeoxyuridine
CCL7	Chemokine CC motif ligand 7
CCN2/CTGF	Cellular communication network factor 2 /connective-tissue growth factor
COL	Collagen
DFCM	Conditioned media
DFs	Dermal fibroblasts
DKK1	Dickkopf 1
DLL	Delta like canonical Notch ligand
dWAT	Dermal white adipose tissue
ECM	Extracellular matrix;
EMT	Epithelial-mesenchymal transition
ENFs	En1-linage negative fibroblasts
EPFs	Engrailed-1-lineage-positive fibroblasts
Fih-1	Factor inhibiting Hif-1α
Foxn1	Forkhead box N1 transcription factor
FRZB	Frizzled-related protein
FZD1 and FZD6	Frizzled Class Receptor 1,6
GFP	Green fluorescent protein
HAS-1	Hyaluronic acid synthase-1
Hif-1α	Hypoxia inducible factor1-alpha
HSP 90	Heat shock protein 90
IGF2	Insulin-like growth factor 2
LC–MS/MS	Liquid chromatography with tandem mass spectrometry
LOX	Lysyl oxidase
LV	Lentiviral vector
MMP	Matrix metalloproteinase
MMPs	Matrix metalloproteinases
NOS 2	Nitric oxide synthase 2
PAI-1(Serpine1)	Plasminogen activator inhibitor-1
PDGFRA	Platelet-derived growth factor receptor A
PKC	Protein kinase C
PLOD2	Procollagen-Lysine, 2-Oxoglutarate 5-Dioxygenase 2
SDC4	Syndecan 4
SFRP2	Secreted frizzled-related protein 2
STAT1	Signal transducer and activator of transcription 1
TGFB-1	Transforming growth factor beta- 1
TGFB-3	Transforming growth factor beta-3
THBS1	Thrombospondin 1
TIMP-1	Tissue inhibitor of metalloproteinase 1, metallopeptidase inhibitor-1
tPA	Tissue-type plasminogen activator
uPA	Urokinase-type plasminogen activator
VEGF	Vascular endothelial growth factor
VLDLR	Very low-density lipoprotein receptor
WPRE	Post-transcriptional regulatory element from woodchuck hepatitis virus
YAP	Yes-associated protein

Supplementary Information

The online version contains supplementary material available at https://doi.org/10.1186/s12915-024-01990-2.

Additional file 1: Table S1. DFs protein regulated upon hypoxia (1% O₂) vs normoxia (21% O₂) that were co-culture with Ad-Foxn1 transduced keratinocytes for 24h. Table S2. DFs protein regulated upon hypoxia (1% O₂) vs normoxia (21% O₂) that were co-culture with Ad-GFP transduced keratinocytes for 24h. Table S3. Dermal fibroblasts conditioned medium (DFCM) protein regulated upon hypoxia (1% O₂) vs normoxia (21% O₂) that were co-culture with Ad-Foxn1 transduced keratinocytes for 24h. Table S4. Dermal fibroblasts conditioned medium (DFCM) protein regulated upon hypoxia (1% O₂) vs normoxia (21% O₂) that were co-culture with Ad-GFP transduced keratinocytes for 24h.

Additional file 2: Figure S1. Classification of DFs proteins regulated upon hypoxia (1% O₂) vs normoxia (21% O₂) that were co-culture with Ad-Foxn1 (A) or Ad-eGFP (B) transduced keratinocytes for 24h according to Gene Ontology (GO) using PANTHER and enriched with g: Profiler database. Diagrams illustrate detected proteins in terms of Biological processes (A), Cellular components (B), Protein class (C) and Pathways (D). Figure S2. Classification of proteins identified in DFCM regulated upon hypoxia (1% O₂) vs normoxia (21% O₂) cultured with keratinocytes transduced with Ad-Foxn1 (A) or Ad-eGFP (B). Diagrams illustrate detected proteins in terms of Biological processes (A), Celluar component (B), Protein class (C) and Molecular Function (D). Figure S3. Full western blots shown in the Fig. 4A. Figure S4. Full western blots shown in the Fig. 4C. Figure S5. Migration ability of Foxn1⁻/⁻ DFs cultured under hypoxia (1% O₂) or normoxia (21% O₂) conditions in KCM (keratinocytes conditioned media) collected from Ad-Foxn1 or Ad-eGFP transduced keratinocytes analyzed within 30hours. Representative photos of wounded DFs (scratch *in vitro* assay). Dotted lines represent edges of the wound. Figure S6. Body weight of Foxn1⁻/⁻ mice treated with LV-eGFP (control), LV-Hif-1α or LV-Foxn1+LV-Hif-1α. Body weight were measured weekly during 4-weeks study (*n*=24 total mice; *n*=8 per treatment). Figure S7. Full western blots shown in the Fig. 11A, Fig. 11B. Figure S8. Full western blots shown in the Fig. 11C, Fig. 11D, Fig. 11E. Figure S9. Full western blots shown in the Fig. 12A. Figure S10. Full western blots shown in the Fig. 12C.

Gawronska-Kozak *et al. BMC Biology*   (2024) 22:193

Page 26 of 28

Authors' contributions

 BGK – designed study/experiments, participated in vitro and in vivo experiments, analysed and interpreted the data, wrote the paper. SMZ – performed in vitro experiments, participated in proteomics analyses, performed western blots, histological staining and examination, participated in data interpretation. KW—performed in vitro experiments, participated in LV construct formation and in vivo experiments, participated in data interpretation. MK – participated in in vivo experiments, performed qRT-PCR analyses, participated in data interpretation. MP – performed proteomics analyses and participated in data interpretation. JW—performed and analysed flow cytometry data, participated in data interpretation.

Availability of data and materials

All data generated or analysed during this study are included in this published article and its supplementary information files, or are available from the corresponding author on reasonable request. The mass spectrometry data have been deposited to Proteomics Identifications Database (PRIDE) with the dataset identifier PXD041939 (36). https://www.ebi.ac.uk/pride/archive/projects/PXD041939.

Declarations

Ethics approval and consent to participate

The experimental animal procedures were approved by the Ethics Committee of the University of Warmia and Mazury (Olsztyn, Poland), No. 68/2018.
All authors read and approved the final manuscript.

Consent for publication

Not applicable.

Competing interests

The authors declare that they have no competing interests.

Author details

[1]Institute of Animal Reproduction and Food Research, Polish Academy of Sciences, Ul. Tuwima 10, 10-748 Olsztyn, Poland. [2]Turku Bioscience Centre, University of Turku and Åbo Akademi University, Tykistökatu 6, Biocity 5 Floor, 20520 Turku, Finland.

References

1. Gurtner GC, Werner S, Barrandon Y, Longaker MT. Wound repair and regeneration. Nature. 2008;453(7193):314–21. Epub 2008/05/16.
2. Gawronska-Kozak B, Bogacki M, Rim JS, Monroe WT, Manuel JA. Scarless skin repair in immunodeficient mice. Wound Repair Regen. 2006;14:265–76.
3. Gawronska-Kozak B. Scarless skin wound healing in FOXN1 deficient (nude) mice is associated with distinctive matrix metalloproteinase expression. Matrix Biol. 2011;30(4):290–300. Epub 2011/05/05.
4. Machcinska S, Kopcewicz M, Bukowska J, Walendzik K, Gawronska-Kozak B. Impairment of the Hif-1alpha regulatory pathway in Foxn1-deficient (Foxn1(-/-)) mice affects the skin wound healing process. FASEB J. 2021;35(2):e21289 Epub 2021/01/22.
5. Corbeaux T, Hess I, Swann JB, Kanzler B, Haas-Assenbaum A, Boehm T. Thymopoiesis in mice depends on a Foxn1-positive thymic epithelial cell lineage. Proc Natl Acad Sci U S A. 2010;107(38):16613–8. Epub 2010/09/09.
6. Brissette JL, Li J, Kamimura J, Lee D, Dotto GP. The product of the mouse nude locus, Whn, regulates the balance between epithelial cell growth and differentiation. Genes Dev. 1996;10(17):2212–21.
7. Mecklenburg L, Tychsen B, Paus R. Learning from nudity: lessons from the nude phenotype. Exp Dermatol. 2005;14(11):797–810.
8. Gawronska-Kozak B, Grabowska A, Kur-Piotrowska A, Kopcewicz M. Foxn1 Transcription Factor Regulates Wound Healing of Skin through Promoting Epithelial-Mesenchymal Transition. PLoS One. 2016;11(3):e0150635 Epub 2016/03/05.
9. Kopcewicz MM, Kur-Piotrowska A, Bukowska J, Gimble JM, Gawronska-Kozak B. Foxn1 and Mmp-9 expression in intact skin and during excisional wound repair in young, adult, and old C57Bl/6 mice. Wound Repair Regen. 2017;25(2):248–59.
10. Walendzik K, Kopcewicz M, Bukowska J, Panasiewicz G, Szafranska B, Gawronska-Kozak B. The Transcription Factor FOXN1 Regulates Skin Adipogenesis and Affects Susceptibility to Diet-Induced Obesity. J Invest Dermatol. 2020;140(6):1166–759 e9 Epub 2019/12/08.
11. Gawronska-Kozak B, Walendzik K, Machcinska S, Padzik A, Kopcewicz M, Wiśniewska J. Dermal White Adipose Tissue (dWAT) is regulated by Foxn1 and Hif-1α during the early phase of skin wound healing. Int J Mol Sci. 2021;23(1):257.
12. Scheid A, Wenger RH, Christina H, Camenisch I, Ferenc A, Stauffer UG, et al. Hypoxia-regulated gene expression in fetal wound regeneration and adult wound repair. Pediatr Surg Int. 2000;16(4):232–6. Epub 2000/07/18.
13. Lokmic Z, Musyoka J, Hewitson TD, Darby IA. Hypoxia and hypoxia signaling in tissue repair and fibrosis. Int Rev Cell Mol Biol. 2012;296:139–85.
14. Sano H, Ichioka S, Sekiya N. Influence of oxygen on wound healing dynamics: assessment in a novel wound mouse model under a variable oxygen environment. PLoS One. 2012;7(11):e50212 Epub 2012/12/05.
15. Kimmel HM, Grant A, Ditata J. The Presence of Oxygen in Wound Healing. Wounds : a compendium of clinical research and practice. 2016;28(8):264–70. Epub 2016/08/26.
16. Li G, Ko CN, Li D, Yang C, Wang W, Yang GJ, et al. A small molecule HIF-1alpha stabilizer that accelerates diabetic wound healing. Nat Commun. 2021;12(1):3363 . Epub 2021/06/09.
17. Hong WX, Hu MS, Esquivel M, Liang GY, Rennert RC, McArdle A, et al. The Role of Hypoxia-Inducible Factor in Wound Healing. Adv Wound Care (New Rochelle). 2014;3(5):390–9. Epub 2014/05/08.
18. Machcinska S, Walendzik K, Kopcewicz M, Wisniewska J, Rokka A, Paakkonen M, et al. Hypoxia reveals a new function of Foxn1 in the keratinocyte antioxidant defense system. FASEB J. 2022;36(8):e22436 Epub 2022/07/07.
19. Driskell RR, Lichtenberger BM, Hoste E, Kretzschmar K, Simons BD, Charalambous M, et al. Distinct fibroblast lineages determine dermal architecture in skin development and repair. Nature. 2013;504(7479):277–81. Epub 2013/12/18.
20. Haydont V, Neiveyans V, Perez P, Busson É, Lataillade J, Asselineau D, et al. Fibroblasts from the human skin dermo-hypodermal junction are distinct from dermal papillary and reticular fibroblasts and from Mesenchymal stem cells and exhibit a specific molecular profile related to extracellular matrix organization and modeling. Cells. 2020;9(2):368.
21. Jiang D, Rinkevich Y. Distinct fibroblasts in scars and regeneration. Curr Opin Genet Dev. 2021;70:7–14. Epub 2021/05/23.
22. Rinkevich Y, Walmsley GG, Hu MS, Maan ZN, Newman AM, Drukker M, et al. Skin fibrosis. Identification and isolation of a dermal lineage with intrinsic fibrogenic potential. Science. 2015;348(6232):aaa2151 Epub 2015/04/18.
23. Jiang D, Correa-Gallegos D, Christ S, Stefanska A, Liu J, Ramesh P, et al. Two succeeding fibroblastic lineages drive dermal development and the transition from regeneration to scarring. Nat Cell Biol. 2018;20(4):422–31. Epub 2018/03/30.

Gawronska-Kozak *et al. BMC Biology*   (2024) 22:193

Page 27 of 28

24. Sorrell JM, Caplan AI. Fibroblast heterogeneity: more than skin deep. J Cell Sci. 2004;117(Pt 5):667–75.

25. Florin L, Hummerich L, Dittrich BT, Kokocinski F, Wrobel G, Gack S, et al. Identification of novel AP-1 target genes in fibroblasts regulated during cutaneous wound healing. Oncogene. 2004;23(42):7005–17. Epub 2004/07/27.

26. Lichtenberger BM, Mastrogiannaki M, Watt FM. Epidermal beta-catenin activation remodels the dermis via paracrine signalling to distinct fibroblast lineages. Nat Commun. 2016;7:10537. Epub 2016/02/04.

27. Mascharak S, desJardins-Park HE, Davitt MF, Griffin M, Borrelli MR, Moore AL, et al. Preventing Engrailed-1 activation in fibroblasts yields wound regeneration without scarring. Science. 2021;372(6540):eaba2374.

28. Mascharak S, Talbott HE, Januszyk M, Griffin M, Chen K, Davitt MF, et al. Multi-omic analysis reveals divergent molecular events in scarring and regenerative wound healing. Cell Stem Cell. 2022;29(2):315–27 e6 Epub 2022/01/26.

29. Gawronska-Kozak B, Kirk-Ballard H. Cyclosporin A reduces matrix metalloproteinases and collagen expression in dermal fibroblasts from regenerative FOXN1 deficient (nude) mice. Fibrogenesis Tissue Repair. 2013;6(1):7 Epub 2013/04/04.

30. Bukowska J, Kopcewicz M, Kur-Piotrowska A, Szostek-Mioduchowska AZ, Walendzik K, Gawronska-Kozak B. Effect of TGFβ1, TGFβ3 and keratinocyte conditioned media on functional characteristics of dermal fibroblasts derived from reparative (Balb/c) and regenerative (Foxn1 deficient; nude) mouse models. Cell Tissue Res. 2018;374(1):149–63.

31. Yusuf F, Gopurappilly R, Dadheech N, Gupta S, Bhonde R, Pal R. Embryonic fibroblasts represent a connecting link between mesenchymal and embryonic stem cells. Dev Growth Differ. 2013;55(3):330–40. Epub 2013/02/28.

32. Fournier BP, Ferre FC, Couty L, Lataillade JJ, Gourven M, Naveau A, et al. Multipotent progenitor cells in gingival connective tissue. Tissue Eng Part A. 2010;16(9):2891–9. Epub 2010/04/24.

33. Leavitt T, Hu MS, Marshall CD, Barnes LA, Lorenz HP, Longaker MT. Scarless wound healing: finding the right cells and signals. Cell Tissue Res. 2016;365(3):483–93. Epub 2016/06/04.

34. Ho S, Marcal H, Foster LJ. Towards scarless wound healing: a comparison of protein expression between human, adult and foetal fibroblasts. Biomed Res Int. 2014;2014:676493 Epub 2014/03/08.

35. Kur-Piotrowska A, Bukowska J, Kopcewicz MM, Dietrich M, Nynca J, Slowinska M, et al. Foxn1 expression in keratinocytes is stimulated by hypoxia: further evidence of its role in skin wound healing. Sci Rep. 2018;8(1):5425 Epub 2018/04/05.

36. Hypoxia and Foxn1 alter the proteomic signature of dermal fibroblasts to redirect scarless wound healing to scar-forming skin wound healing in Foxn1-/- mice. 2024. PRIDE, EMBL-EBI accession: PXD041939. https://www.ebi.ac.uk/pride/archive/projects/PXD041939.

37. Estes JM, Adzick NS, Harrison MR, Longaker MT, Stern R. Hyaluronate metabolism undergoes an ontogenic transition during fetal development: implications for scar-free wound healing. J Pediatr Surg. 1993;28(10):1227–31.

38. Coelho PGB, Souza MV, Conceicao LG, Viloria MIV, Bedoya SAO. Evaluation of dermal collagen stained with picrosirius red and examined under polarized light microscopy. An Bras Dermatol. 2018;93(3):415–8. Epub 2018/06/21.

39. Caskey RC, Allukian M, Lind RC, Herdrich BJ, Xu J, Radu A, et al. Lentiviral-mediated over-expression of hyaluronan synthase-1 (HAS-1) decreases the cellular inflammatory response and results in regenerative wound repair. Cell Tissue Res. 2013;351(1):117–25. Epub 2012/11/15.

40. Kuhn U, Terunuma A, Pfutzner W, Foster RA, Vogel JC. In vivo assessment of gene delivery to keratinocytes by lentiviral vectors. J Virol. 2002;76(3):1496–504. Epub 2002/01/05.

41. Woodley DT, Keene DR, Atha T, Huang Y, Ram R, Kasahara N, et al. Intradermal injection of lentiviral vectors corrects regenerated human dystrophic epidermolysis bullosa skin tissue in vivo. Mol Ther. 2004;10(2):318–26. Epub 2004/08/06.

42. Ghazizadeh S, Katz AB, Harrington R, Taichman LB. Lentivirus-mediated gene transfer to human epidermis. J Investig Dermatol Symp Proc. 2004;9(1):269–75. Epub 2004/09/17.

43. Kunicher N, Falk H, Yaacov B, Tzur T, Panet A. Tropism of lentiviral vectors in skin tissue. Hum Gene Ther. 2008;19(3):255–66. Epub 2008/02/22.

44. Nanba D, Matsushita N, Toki F, Higashiyama S. Efficient expansion of human keratinocyte stem/progenitor cells carrying a transgene with lentiviral vector. Stem Cell Res Ther. 2013;4(5):127 Epub 2014/01/11.

45. Jakobsen M, Askou AL, Stenderup K, Rosada C, Dagnaes-Hansen F, Jensen TG, et al. Robust Lentiviral Gene Delivery But Limited Transduction Capacity of Commonly Used Adeno-Associated Viral Serotypes in Xenotransplanted Human Skin. Hum Gene Ther Methods. 2015;26(4):123–33. Epub 2015/07/24.

46. Botusan IR, Sunkari VG, Savu O, Catrina AI, Grünler J, Lindberg S, et al. Stabilization of HIF-1α is critical to improve wound healing in diabetic mice. Proc Natl Acad Sci USA. 2008;105(49):19426–31.

47. Deschene K, Celeste C, Boerboom D, Theoret CL. Hypoxia regulates the expression of extracellular matrix associated proteins in equine dermal fibroblasts via HIF1. J Dermatol Sci. 2012;65(1):12–8. Epub 2011/10/18.

48. Xue M, Jackson CJ. Extracellular Matrix Reorganization During Wound Healing and Its Impact on Abnormal Scarring. Adv Wound Care (New Rochelle). 2015;4(3):119–36. Epub 2015/03/19.

49. Lu P, Takai K, Weaver VM, Werb Z. Extracellular matrix degradation and remodeling in development and disease. Cold Spring Harb Perspect Biol. 2011;3(12):a005058.

50. Zhang L, Yaron JR, Tafoya AM, Wallace SE, Kilbourne J, Haydel S, et al. A virus-derived immune modulating Serpin accelerates wound closure with improved collagen remodeling. J Clin Med. 2019;8(10):1626.

51. Freeberg MAT, Easa A, Lillis JA, Benoit DSW, van Wijnen AJ, Awad HA. Transcriptomic Analysis of Cellular Pathways in Healing Flexor Tendons of Plasminogen Activator Inhibitor 1 (PAI-1/Serpine1) Null Mice. J Orthop Res. 2020;38(1):43–58. Epub 2019/08/20.

52. Zou ML, Teng YY, Chen ZH, Liu SY, Jia Y, Zhang KW, et al. The uPA System Differentially Alters Fibroblast Fate and Profibrotic Ability in Skin Fibrosis. Front Immunol. 2022;13:845956. Epub 2022/04/05

53. Liu RM. Oxidative stress, plasminogen activator inhibitor 1, and lung fibrosis. Antioxid Redox Signal. 2008;10(2):303–19. Epub 2007/11/06.

54. Huang EY, Wu H, Island ER, Chong SS, Warburton D, Anderson KD, et al. Differential expression of urokinase-type plasminogen activator and plasminogen activator inhibitor-1 in early and late gestational mouse skin and skin wounds. Wound Repair Regen. 2002;10(6):387–96. Epub 2002/11/28.

55. Island E, Wu H, Warburton D, Anderson K, Tuan TL. Developmental differences in the expression and modulation of extracellular matrix proteases and inhibitors in mouse skin fibroblasts. Wound Repair Regen. 1999;7(6):467–76. Epub 2000/01/13.

56. Kong HJ, Kwon EJ, Kwon OS, Lee H, Choi JY, Kim YJ, et al. Crosstalk between YAP and TGFbeta regulates SERPINE1 expression in mesenchymal lung cancer cells. Int J Oncol. 2021;58(1):111–21. Epub 2020/12/29.

57. Nilsson L, Gafvels M, Musakka L, Ensler K, Strickland DK, Angelin B, et al. VLDL activation of plasminogen activator inhibitor-1 (PAI-1) expression: involvement of the VLDL receptor. J Lipid Res. 1999;40(5):913–9. Epub 1999/05/01.

58. Kur-Piotrowska A, Kopcewicz M, Kozak LP, Sachadyn P, Grabowska A, Gawronska-Kozak B. Neotenic phenomenon in gene expression in the skin of Foxn1- deficient (nude) mice - a projection for regenerative skin wound healing. BMC Genomics. 2017;18(1):56.

59. Lee YS, Wysocki A, Warburton D, Tuan TL. Wound healing in development. Birth Defects Res C Embryo Today. 2012;96(3):213–22. Epub 2012/10/31.

60. Hu B, Lefort K, Qiu W, Nguyen BC, Rajaram RD, Castillo E, et al. Control of hair follicle cell fate by underlying mesenchyme through a CSL-Wnt5a-FoxN1 regulatory axis. Genes Dev. 2010;24(14):1519–32. Epub 2010/07/17.

61. Lee MJ, Byun MR, Furutani-Seiki M, Hong JH, Jung HS. YAP and TAZ regulate skin wound healing. J Invest Dermatol. 2014;134(2):518–25. Epub 2013/10/11.

62. Moya IM, Halder G. Hippo-YAP/TAZ signalling in organ regeneration and regenerative medicine. Nat Rev Mol Cell Biol. 2019;20(4):211–26. Epub 2018/12/14.

63. Zhang H, Pasolli HA, Fuchs E. Yes-associated protein (YAP) transcriptional coactivator functions in balancing growth and differentiation in skin. Proc Natl Acad Sci U S A. 2011;108(6):2270–5. Epub 2011/01/26.

64. Elbediwy A, Vincent-Mistiaen ZI, Spencer-Dene B, Stone RK, Boeing S, Wculek SK, et al. Integrin signalling regulates YAP and TAZ to control skin homeostasis. Development. 2016;143(10):1674–87. Epub 2016/03/19.

Gawronska-Kozak *et al. BMC Biology*   (2024) 22:193

Page 28 of 28

65. Liu F, Lagares D, Choi KM, Stopfer L, Marinkovic A, Vrbanac V, et al. Mechanosignaling through YAP and TAZ drives fibroblast activation and fibrosis. Am J Physiol Lung Cell Mol Physiol. 2015;308(4):L344–57. Epub 2014/12/17.

66. Islam MS, Parish M, Brennan JT, Winer BL, Segars JH. Targeting fibrotic signaling pathways by EGCG as a therapeutic strategy for uterine fibroids. Sci Rep. 2023;13(1):8492 Epub 2023/05/26.

67. Kanehisa M, Goto S. KEGG: kyoto encyclopedia of genes and genomes. Nucleic Acids Res. 2000;28(1):27–30. Epub 1999/12/11.

68. Szklarczyk D, Gable AL, Lyon D, Junge A, Wyder S, Huerta-Cepas J, et al. STRING v11: protein-protein association networks with increased coverage, supporting functional discovery in genome-wide experimental datasets. Nucleic Acids Res. 2019;47(D1):D607–13. Epub 2018/11/27.

69. Shannon P, Markiel A, Ozier O, Baliga NS, Wang JT, Ramage D, et al. Cytoscape: a software environment for integrated models of biomolecular interaction networks. Genome Res. 2003;13(11):2498–504. Epub 2003/11/05.

70. Graham FL, van der Eb AJ. A new technique for the assay of infectivity of human adenovirus 5 DNA. Virology. 1973;52(2):456–67.

Publisher's Note